

Density-functional-theory approach to the thermodynamics of the harmonically confined one-dimensional Hubbard model

V. L. Campo*

*Departamento de Física, Universidade Federal de São Carlos, Rodovia Washington Luís, km 235,
Caixa Postal 676, 13565-905 São Carlos, SP, Brazil*

(Received 24 July 2014; published 13 July 2015)

The thermodynamics of the inhomogeneous one-dimensional repulsive fermionic Hubbard model with parabolic confinement is studied by a density-functional-theory approach, based on Mermin's generalization to finite temperatures. A local-density approximation (LDA), based on exact results for the homogeneous model, is used to approximate the correlation part in the Helmholtz free-energy, comprising the thermodynamic Bethe ansatz LDA (TBALDA). The general presentation of the method is given and some properties of the homogeneous model that are relevant to the DFT approach are analyzed. Extensive comparison between TBALDA and numerical exact diagonalization results for thermodynamic properties of small inhomogeneous chains is discussed. In the remaining, a classical thermodynamic treatment of the confined system is developed with the focus on global properties of large systems. It is observed that, depending on the temperature and specific volume, the system can have its temperature increased under isentropic expansion. Such unusual behavior becomes more pronounced with the increase of the intrasite interaction U and can be understood considering the peculiar behavior of the correlation entropy per site of the Hubbard model around half-filling. A related nonmonotonic variation of the temperature under isentropic change of U is also studied. At the end, the dependence of the double occupancy on temperature and volume per particle is discussed.

DOI: [10.1103/PhysRevA.92.013614](https://doi.org/10.1103/PhysRevA.92.013614)

PACS number(s): 03.75.Ss, 67.85.Lm, 05.30.Fk

I. INTRODUCTION

Ab initio calculations based on density-functional theory (DFT) [1] have become more and more popular in the last 30 years thanks to the continuous improvement on energy functionals, algorithms, and available computational resources, with definitive impact on chemistry, physics, and materials science. The original formulation by Hohenberg and Kohn [2] was devised to the ground-state electronic density, however, applications in solid state physics and materials science usually demand that temperature be taken into account appropriately. Soon after the foundation of DFT by Hohenberg and Kohn, Mermin [3] generalized the formulation to the finite temperature case. The contribution of phonons to the thermodynamic properties of the system is absent from Mermin's formulation, but phonon spectra can be computed within DFT [4] and their contribution to the physical properties can be incorporated [4,5]. Alternative approaches are under the umbrella of *ab initio* molecular dynamics [6–8]. Accurate computation of the thermodynamic properties of materials at extreme conditions has had impact in the study of Earth's mantle [9] and in the study of warm dense matter [10] for example. In applied physics, very complex systems, as many-components steels [11], have also been successfully approached by DFT. Recent quantum Monte Carlo numerical results for the temperature dependence of the exchange-correlation energy of the homogeneous electron gas [12] and the proposed analytical fitting to this dependence [13] will certainly allow improvement in the free-energy functionals.

In the last decade, DFT has been used to study model systems, such as the Hubbard model, the Heisenberg model, and

other models [14]. The work for model systems has progressed similarly to the work in DFT to study realistic systems. Starting from ground-state DFT with simple functionals, there has been progress in functional development and in the extension to treat time-dependent situations, but almost no work has been dedicated to treat systems at finite temperature. We mention here an application of DFT to the single impurity Kondo model [15] and the pioneering work by Xianlong *et al.* [16] on the one-dimensional (1D) fermionic repulsive Hubbard model, where the same approach of the present paper was discussed but implemented in a different way, by means of an approximate parametrization for the correlation energy. In this work the correlation energy and its derivatives are obtained directly from the exact solution of the homogeneous model.

The inhomogeneous fermionic Hubbard model can describe quite well systems of trapped ultracold atoms in optical lattices [17]. Actually, one important motivation to build such ultracold atomic systems is to investigate experimentally the Hubbard model properties [18,19], given the relevance of the model to condensed matter physics and the fact that, despite 50 years of theoretical work, its physical properties remain only partially understood in two and three dimensions. In ultracold atomic systems, some external potential has to be present to confine the atoms, giving rise to inhomogeneous systems, promoting the approach to them by DFT, which will benefit from the fact that both the lattice and the confining potential are fixed, so that Mermin's formulation can be directly used here.

In this work, the thermodynamics of the one-dimensional repulsive fermionic Hubbard model under parabolic confinement is obtained from a DFT approach according to Mermin's formulation. The correlation Helmholtz free-energy is approximated by the local-density approximation (LDA) based on exact results for the homogeneous model in the thermodynamic limit [20–25], which is a natural extension

*vivaldo.leiria@gmail.com, vlcampo@df.ufscar.br

to finite temperatures of the Bethe ansatz LDA (BALDA) used to treat the inhomogeneous Hubbard model at $T = 0$ K [14]. For $T > 0$ K, the approximation will be called here thermal Bethe ansatz LDA, or simply TBALDA. In the same way the homogeneous electron gas is the reference system to build the LDA used in *ab initio* calculations [1], the homogeneous Hubbard model is the reference system to build the BALDA and the TBALDA used here. The adoption of this reference system is crucial to the success of BALDA to treat the inhomogeneous Hubbard model [14]. Within BALDA, not only the energy of the homogeneous system is exact, but also the energy gap in the charge sector of the half-filled homogeneous system is exactly taken into account [14]. This energy gap is entirely due to the on-site interaction and makes the half-filled system insulating. In confined inhomogeneous systems, this energy gap is the reason for the coexistence of an insulating phase (corresponding to a plateau with density equal to one in the density profile) and a surrounding metallic phase [26,27].

Despite the inhomogeneity of this confined one-dimensional system, it is presented here a definition for its volume. What follows is that the thermodynamic behavior of the confined system can be described in the same way we do for homogeneous systems, having temperature, chemical potential, and volume as independent variables. The inhomogeneity becomes apparently hidden, but has direct consequences for the thermodynamic behavior as it is shown in the present analysis of isentropic transformations. Isentropic transformations are naturally motivated by the experimental situation, where ultracold atomic systems are thermally isolated and the confining potential can be tuned. It is found here that in narrow ranges of specific volume and temperature, the temperature in fact increases under isentropic expansion. This interesting behavior is linked to the changes that happen in the density profile as the confinement is relaxed and it is shown that it can be understood, in the framework of TBALDA, as a direct consequence of the peculiar density dependence of the correlation entropy in the homogeneous Hubbard model at low temperatures. This unusual behavior becomes more pronounced increasing the intrasite interaction.

The work is organized as follows: Sec. II presents the model Hamiltonian and Mermin's formulation to the model system is discussed in detail, Sec. III explains the thermodynamic Bethe ansatz local-density approximation (TBALDA) used for the correlation Helmholtz free-energy, Sec. IV discusses some properties of the homogeneous systems that are relevant to the DFT approach, and Sec. V presents a careful comparison between DFT results based on TBALDA and exact results for a short chain, where the approach can be seen to work well in spite of the smallness of the chain. A brief comparison with DMRG results for larger chains is also showed. In Sec. VI the thermodynamics of the harmonically confined Hubbard model is obtained from DFT calculations and a detailed study of the behavior of the system under isentropic transformations is presented. We discuss two possible transformations: changes of the volume with constant intrasite interaction and changes of the intrasite interaction with constant volume. We finish the section discussing the behavior of the double occupancy. The conclusion follows in Sec. VII.

II. BACKGROUND ON DENSITY-FUNCTIONAL THEORY: MERMIN'S THEOREM AND KOHN-SHAM SCHEME

Consider a system described by the one-dimensional fermionic Hubbard model in the presence of an external potential, at fixed temperature (T) and chemical potential (μ). The system Hamiltonian is given by

$$\hat{H} = \hat{K} + \hat{U} + \sum_j v_j \hat{n}_j, \quad (1)$$

$$\hat{K} = -t \sum_{j,\sigma} (c_{j,\sigma}^\dagger c_{j+1,\sigma} + \text{H.c.}), \quad (2)$$

$$\hat{U} = U \sum_j \hat{n}_{j,\uparrow} \hat{n}_{j,\downarrow}. \quad (3)$$

$c_{j,\sigma}^\dagger$ creates a fermion at site j with spin z -component $\sigma (= \pm 1/2)$, $\hat{n}_{j,\sigma} = c_{j,\sigma}^\dagger c_{j,\sigma}$ is the spin-resolved site occupation operator at site j , and $\hat{n}_j = \hat{n}_{j,\uparrow} + \hat{n}_{j,\downarrow}$ is the total site occupation operator at site j . \hat{K} represents the kinetic energy in this tight-binding model with hopping integral t . \hat{U} represents the interaction energy operator, which increases by U the energy of any doubly occupied site. The external potential has amplitude v_j at site j and couples directly to the density. Hereafter we will express any energy in units of the hopping integral t .

Mermin's theorem [3] is the generalization of Hohenberg and Kohn theorem [1,2] to the case of fixed temperature and chemical potential, establishing the one-to-one correspondence between the external potential and the electronic density. Both theorems were originally established for continuous electronic systems with Coulomb interaction in mind. However, their generalization to discrete systems as the Hubbard model does not pose any difficulty. In this case, there is a one-to-one correspondence between the external potential set $\{v_j\}$ and the equilibrium site-occupations set $\{n_j\}$. For simplicity and to reinforce the parallelism with the continuous case, we will refer to site occupations as densities.

Let us briefly remind the reader of the main aspects of Mermin's theorem [3]. The thermodynamic properties of the system described by the Hamiltonian in Eq. (1) are determined by the equilibrium density-matrix

$$\hat{\rho}_{\text{eq}} = \frac{e^{-\beta(\hat{H} - \mu\hat{N})}}{\text{Tr}\{e^{-\beta(\hat{H} - \mu\hat{N})}\}}, \quad (4)$$

which is the density matrix that minimizes the functional

$$\Omega[\hat{\rho}] = \text{Tr}\{\hat{\rho}[\hat{H} + k_B T \ln(\hat{\rho}) - \mu\hat{N}]\}. \quad (5)$$

At equilibrium, $\Omega[\hat{\rho}_{\text{eq}}]$ is nothing else than the grand canonical potential,

$$\Omega[\rho_{\text{eq}}] = E - TS - \mu N = -k_B T \ln(Z_G), \quad (6)$$

where E is the internal energy, S is the entropy, N is the number of particles, and

$$Z_G = \text{Tr}\{e^{-\beta(\hat{H} - \mu\hat{N})}\} \quad (7)$$

is the grand partition function.

From the minimizing property of $\hat{\rho}_{\text{eq}}$, Mermin proved the one-to-one correspondence between the external potential and the equilibrium density in the same way as Hohenberg and

Kohn, based on the minimizing property of the ground-state wave function, proved such correspondence for an isolated system at $T = 0$.

Since the density determines the external potential and the external potential determines $\hat{\rho}_{\text{eq}}$, we can introduce the universal density functional

$$\mathcal{F}[n](\mu, T) = \text{Tr}\{\hat{\rho}_{\text{eq}}[n][\hat{K} + \hat{U} + k_B T \ln(\hat{\rho}_{\text{eq}}[n])]\}, \quad (8)$$

with no explicit reference to the external potential, which is itself a functional of the density. Following Mermin, for fixed T and μ and for a given external potential, we define the density functional

$$\Omega_v[n](\mu, T, U) \equiv \mathcal{F}[n](\mu, T, U) - \mu N + \sum_j v_j n_j \quad (9)$$

and note that this functional is minimized by the equilibrium density

$$n_j^{\text{eq}} = \text{Tr}\{\hat{\rho}_{\text{eq}} \hat{n}_j\}, \quad (10)$$

opening the door to make a variational approach to determine the equilibrium density along the lattice as well as the thermodynamic properties of the system. The equilibrium density is the minimum point of $\Omega_v[n](T, \mu, U)$, therefore

$$\frac{\partial \mathcal{F}}{\partial n_j}[n_{\text{eq}}] + v_j - \mu = 0, \quad \text{any } j. \quad (11)$$

The main difficulty is that the universal functional $\mathcal{F}[n](\mu, T)$ is not exactly known and some approximation to it is required to move on. Before considering the approximation to be used, let us make some remarks about the thermodynamics quantities of interest here.

For the equilibrium density, the functional $\Omega_v[n_{\text{eq}}]$ gives the grand canonical potential and $\Omega_v[n_{\text{eq}}] + \mu N$ gives the Helmholtz free-energy. Two other quantities of interest are the entropy and the number of doubly occupied sites

$$N_D = \text{Tr} \left\{ \hat{\rho}_{\text{eq}} \sum_j \hat{n}_{j,\uparrow} \hat{n}_{j,\downarrow} \right\} = \text{Tr} \left\{ \hat{\rho}_{\text{eq}} \frac{\hat{U}}{U} \right\}. \quad (12)$$

The entropy is given by $-(\frac{\partial \Omega}{\partial T})_{\mu, U}$. When differentiating Eq. (9) with respect to the temperature, it is important to take into account that the site occupations depend on the temperature, so

$$-S(\mu, T, U) = \sum_j \left[\frac{\partial \mathcal{F}}{\partial n_j}[n_{\text{eq}}](\mu, T, U) + v_j - \mu \right] \left(\frac{\partial n_j}{\partial T} \right) + \frac{\partial \mathcal{F}}{\partial T}[n_{\text{eq}}](\mu, T, U), \quad (13)$$

and from Eq. (11) we have

$$-S(\mu, T, U) = \frac{\partial \mathcal{F}}{\partial T}[n_{\text{eq}}](\mu, T, U). \quad (14)$$

Here we have energies in units of t , temperature in units of t/k_B , and entropy in units of k_B .

For the number of doubly occupied sites, considering eigenstates of the Hamiltonian to compute the trace in (12) and the Hellmann-Feynman theorem, it is straightforward to

get

$$N_D = \left(\frac{\partial \Omega}{\partial U} \right)_{\mu, T}. \quad (15)$$

Differentiating Eq. (9) with respect to U at the equilibrium density, we find

$$N_D = \frac{\partial \mathcal{F}}{\partial U}[n_{\text{eq}}](\mu, T, U). \quad (16)$$

According to the Kohn-Sham scheme, an auxiliary system of noninteracting fermions is considered with the requirement that its density be exactly the same as the density in the interacting system. This auxiliary noninteracting system is usually called the Kohn-Sham system. The universal functional for the interacting system will be decomposed as follows:

$$\mathcal{F}[n](\mu, T, U) \equiv \mathcal{F}_0[n](\mu, T) + E_{\text{Hartree}}[n](U) + \mathcal{F}_c[n](\mu, T, U). \quad (17)$$

The first term on the right-hand side of (17) is the universal functional for the noninteracting system ($U = 0$), $\mathcal{F}_0[n](\mu, T) = F[n](T, \mu, 0)$. The second term is the Hartree energy, here defined as

$$E_{\text{Hartree}}[n](U) = \frac{U}{4} \sum_j n_j^2, \quad (18)$$

corresponding to the first-order (in U) approximation to the expected value of \hat{U} . The third term, $\mathcal{F}_c[n](\mu, T, U)$, is the correlation energy functional, which encompasses all the subtle many-body features of the universal functional.

It is important to note that the correlation functional does not come only from the difference between the Hartree energy and the interacting energy (\hat{U}), but has a contribution due to the difference between the kinetic energy of the interacting system and the kinetic energy of the noninteracting system, as well as a contribution due to the difference between the entropies of these systems. In traditional DFT, the many-body term is referred to as exchange-correlation functional, but because the Hubbard model with one level per site does not have exchange energy, we use only correlation here.

With the decomposition in Eq. (17), the functional to be minimized [Eq. (9)] is written as

$$\Omega_v[n](\mu, T, U) = \mathcal{F}_0[n](\mu, T) + \frac{U}{4} \sum_j n_j^2 + \mathcal{F}_c[n](\mu, T, U) + \sum_j v_j n_j - \mu N. \quad (19)$$

At the exact density we have $\frac{\partial \Omega_v[n](\mu, T, U)}{\partial n_j} = 0$ for any j , which implies

$$\frac{\partial \mathcal{F}_0[n](\mu, T)}{\partial n_j} + \frac{U}{2} n_j + \frac{\partial \mathcal{F}_c[n](\mu, T, U)}{\partial n_j} + v_j - \mu = 0. \quad (20)$$

Defining the correlation potential by

$$v_j^c = \frac{\partial \mathcal{F}_c[n](\mu, T, U)}{\partial n_j}, \quad (21)$$

and the Kohn-Sham potential by

$$v_j^{\text{KS}} = v_j + \frac{U}{2}n_j + v_j^c, \quad (22)$$

Eq. (20) becomes equivalent to

$$\frac{\partial \mathcal{F}_0[n](\mu, T)}{\partial n_j} + v_j^{\text{KS}} - \mu = 0, \quad (23)$$

which is exactly the equation we would have for a noninteracting system with chemical potential μ in the presence of an external potential given by v^{KS} .

For a given Kohn-Sham potential v^{KS} , we can solve the noninteracting problem set by Eq. (23) determining the single-particle states and populating them according to the Fermi-Dirac distribution. In particular, the density for the Kohn-Sham system will be given by

$$n_j^{\text{KS}} = \sum_l \frac{1}{e^{\beta(\epsilon_l - \mu)} + 1} \langle \varphi_l | \hat{n}_j | \varphi_l \rangle, \quad (24)$$

where the sum runs over all the single-particle states $|\varphi_l\rangle$ with corresponding energies ϵ_l .

However, the Kohn-Sham potential is a functional of the density [see Eqs. (21) and (22)]. For a given external potential, we minimize the functional $\Omega_v[n]$ in Eq. (19) starting with a trial density n^0 . From n^0 , we compute v^{KS} , solve the noninteracting problem, and determine its density n^1 by Eq. (24). If $n^1 \neq n^0$, a new trial density based on n^0 and n^1 is suggested and the procedure is repeated until convergence. This is the self-consistent Kohn-Sham scheme. The whole procedure would be exact if the correlation functional and its derivative were exactly known. With an approximate correlation functional, the Kohn-Sham scheme will give an approximation to the density, to the grand canonical potential, and to other properties.

III. TBALDA

Here we will make the local-density approximation to the correlation energy. It is based on the exact Helmholtz free-energy per site for the homogeneous Hubbard model with no external potential in the thermodynamic limit. This approximation will be referred to as thermodynamic Bethe ansatz local-density approximation, or more simply, as TBALDA. There are two main approaches to calculate the thermodynamic properties of the homogeneous Hubbard model. The first one, due to Takahashi [20–22], is the one known as thermodynamic Bethe ansatz. This approach leads to an infinite set of equations, which nonetheless can be treated numerically to reasonable accuracy [22]. The second approach is based on the quantum transfer matrix (QTM) method to deal with integrable systems and was formulated more recently [23–25]. The QTM approach leads to a finite (and small) set of integral equations and was the approach followed by me to compute the properties of the homogeneous model, although the denomination used here suggests the opposite. The main reason to adopt this denomination is to make clear that the present work is a

natural extension of previous work in density-functional theory applied to the Hubbard model [14,28–30], where the acronym BALDA has become well established.

The local-density approximation will be used in combination with the Kohn-Sham scheme [1,31] to approximate only the correlation part $\mathcal{F}_c[n](\mu, T, U)$ of the universal functional in Eq. (8). We have

$$\mathcal{F}_c[n](\mu, T, U) \approx \sum_j f_c(n_j, T, U), \quad (25)$$

where $f_c(n_j, T, U)$ is the Helmholtz correlation energy per site of a homogeneous system in the thermodynamic limit with site occupation n_j . According to Eq. (17), f_c is given by

$$f_c(n, T, U) = f(n, T, U) - f_0(n, T) - \frac{U}{4}n^2, \quad (26)$$

where $f(n, T, U)$ and $f_0(n, T)$ are the Helmholtz free-energies per site in the interaction and noninteracting systems, respectively. Therefore, within LDA, a generic site j of the real inhomogeneous system contributes to \mathcal{F}_c as it would contribute if it were part of an infinite homogeneous lattice with density equal to n_j everywhere.

On the right-hand side of Eq. (25), the dependence on the chemical potential has disappeared and this deserves clarification. The point is that the reference infinite homogeneous system is considered with external potential *equal to zero*. If in the real system the site j has occupation n_j , we need to consider a homogeneous system with site occupation equal to n_j at all sites. In this homogeneous system, the chemical potential must be equal to $\mu(n_j, T, U) = \left(\frac{\partial f}{\partial n}\right)_{T,U}(n_j, T, U)$, where f is the Helmholtz free-energy per site for the homogeneous system. Alternatively, one could keep the chemical potential of the real system as an argument of f_c in (25), provided that the possibility of adding a uniform external potential \tilde{v} to the homogeneous system was allowed. But this uniform external potential is equivalent to a shift in the chemical potential. When $\mu - \tilde{v} = \mu(n_j, T, U)$, we would have a system with site occupation n_j .

The one-to-one correspondence between the chemical potential and the site occupation for the homogeneous system is illustrated in Fig. 1 for different temperatures and Us . Additionally, the derivative of density with respect to the chemical potential as a function of the density is displayed in Fig. 2 for several temperatures and $U = 8$.

Solving the integral equations coming from the QTM method, we determine $f(n, T, U)$. For $U = 0$ it is simpler to make a direct calculation to get

$$f_0(n, T) = -\frac{2k_B T}{\pi} \int_0^\pi \ln(1 + e^{-\beta(\epsilon_k - \mu_0)}) dk + \mu_0 n. \quad (27)$$

The single-particle energy is given by $\epsilon_k = -2t \cos(k)$ and the noninteracting chemical potential μ_0 is an implicit function of the density n through the relation

$$n = \frac{2}{\pi} \int_0^\pi \frac{1}{e^{\beta(\epsilon_k - \mu_0)} + 1} dk, \quad (28)$$

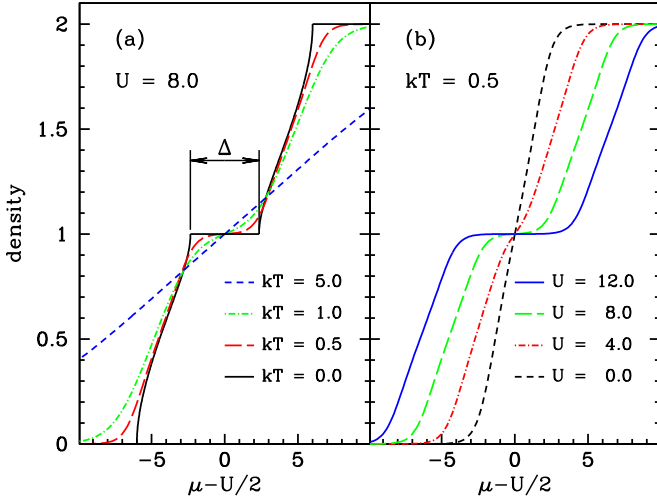


FIG. 1. (Color online) Density as a function of the chemical potential for the homogeneous one-dimensional Hubbard model. Energies are in units of the hopping parameter t [Eq. (1)]. The system is half-filled ($n = 1$) when $\mu = U/2$. In this case, the system is insulating at $T = 0$ and the density as a function of the chemical potential is constant and equal to one for $\frac{U}{2} - \frac{\Delta}{2} \leq \mu \leq \frac{U}{2} + \frac{\Delta}{2}$, where Δ is the energy gap in the charge sector. For $U = 8.0$, $\Delta \approx 4.6795$. When the temperature is small compared to Δ , the above mentioned plateau is apparent.

where the Fermi-Dirac occupations for all extended single-particle states are added to build the total density.

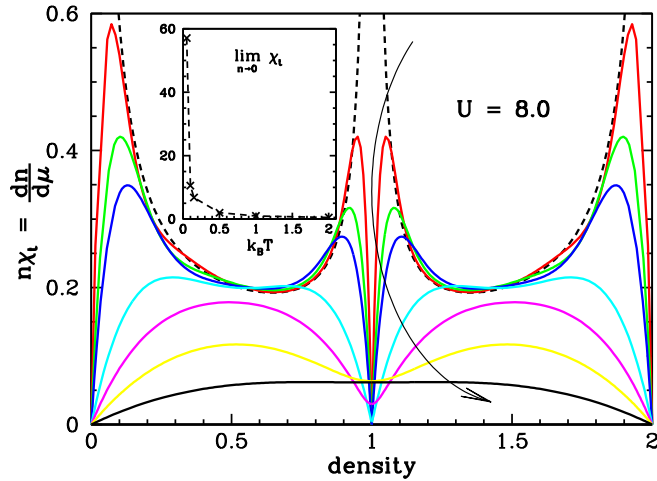


FIG. 2. (Color online) Density times the charge susceptibility [as defined in Eq. (56)] as a function of the density for the homogeneous system with $U = 8.0$ at several temperatures. The dashed line corresponds to $k_B T = 0$. The charge susceptibility diverges as the density approaches 0, 1, and 2, but if the density is exactly equal to one of these values, the charge susceptibility is equal to zero, as it is clear from Fig. 1. The other lines correspond to $k_B T = 0.05, 0.10, 0.15, 0.5, 1.0, 2.0,$ and 5.0 in the order the arrow crosses them. In the inset we have the charge susceptibility in the limit of zero density. The finite value of this limit shows that $(\frac{\partial n}{\partial \mu})_T$ behaves linearly with the density as $n \rightarrow 0$.

From the approximate correlation functional, we obtain the approximate correlation potential as follows:

$$\begin{aligned} v_j^c &= \frac{\partial \mathcal{F}_c^{\text{LDA}}}{\partial n_j} = \frac{\partial f_c}{\partial n_j}(n_j, T, U) \\ &= \mu(n_j, T, U) - \mu_0(n_j, T) - \frac{U}{2} n_j, \end{aligned} \quad (29)$$

where the chemical potential for the interacting homogeneous system is also obtained from integral equations coming from the QTM method, while for the noninteracting system it is given by the implicit function in (28). Accordingly, the Kohn-Sham potential at site j [Eq. (22)] will be given by

$$v_j^{\text{KS}} = v_j + \mu(n_j, T, U) - \mu_0(n_j, T). \quad (30)$$

After convergence of the self-consistent Kohn-Sham scheme, we end up with an approximation to the density profile along the real interacting system. This density is the same as the density in the auxiliary noninteracting system. The grand canonical potential can be promptly determined from Eqs. (9), (17), (18), and (25),

$$\begin{aligned} \Omega_v[n_{\text{eq}}](\mu, T, U) &= \mathcal{F}_0[n_{\text{eq}}](\mu, T) + \sum_j \frac{U}{4} n_j^2 \\ &+ \sum_j f_c(n_j, T, U) + \sum_j (v_j - \mu) n_j, \end{aligned} \quad (31)$$

where

$$\mathcal{F}_0[n_{\text{eq}}](\mu, T) = \text{Tr}\{\hat{\rho}_0[\hat{K} + k_B T \ln(\hat{\rho}_0)]\} \quad (32)$$

and $\hat{\rho}_0$ is the equilibrium density matrix for the noninteracting auxiliary system, whose single-particle energies are known and can be used to write

$$\begin{aligned} \mathcal{F}_0[n_{\text{eq}}](\mu, T) &= -k_B T \sum_l \ln(1 + e^{-(\epsilon_l - \mu)/k_B T}) \\ &- \sum_j (v_j^{\text{KS}} - \mu) n_j. \end{aligned} \quad (33)$$

In the first sum, l runs over the single-particle states, while in the second sum, j runs over the sites. Substituting Eq. (33) back into Eq. (31) we get

$$\begin{aligned} \Omega_v(\mu, T, U) &= -k_B T \sum_l \ln(1 + e^{-(\epsilon_l - \mu)/k_B T}) \\ &+ \sum_j \left(v_j - v_j^{\text{KS}} + \frac{U}{4} n_j \right) n_j \\ &+ \sum_j f_c(n_j, T, U). \end{aligned} \quad (34)$$

In the same way we related the entropy of the interacting system to the derivative of its universal functional with respect to the temperature [Eq. (14)], we have the following relation for the noninteracting Kohn-Sham system:

$$-S_{\text{KS}}(\mu, T) = \frac{\partial \mathcal{F}_0}{\partial T}[n_{\text{eq}}](\mu, T). \quad (35)$$

Therefore, the entropy can be computed differentiating Eq. (17). Within TBALDA for the correlation energy we get

$$\begin{aligned} & -S(\mu, T, U) \\ &= \sum_j \left[\frac{\partial \mathcal{F}_0}{\partial n_j} [n_{\text{eq}}] + \frac{U}{2} n_j + v_j^c + v_j - \mu \right] \frac{\partial n_j}{\partial T} \\ &+ \frac{\partial \mathcal{F}_0}{\partial T} [n_{\text{eq}}] - \sum_j [s(n, T, U) - s_0(n, T)]. \end{aligned} \quad (36)$$

From the Euler equation (23), the term between square brackets in the first sum vanishes. From (35) we have

$$S(\mu, T, U) = S_{\text{KS}}(\mu, T) + \sum_j [s(n, T, U) - s_0(n, T)]. \quad (37)$$

Analogously, for the number of doubly occupied sites, we have, within TBALDA,

$$N_D = \sum_j \frac{\partial f}{\partial U}(n_j, T, U). \quad (38)$$

For situations when the number of particles is fixed, we proceed with the canonical ensemble formalism. The adaptation of the previous formulation is straightforward. Instead of the grand canonical potential, we have the Helmholtz free-energy. The universal functional is defined in the same way as done in Eq. (8), but with the densities satisfying the constraint of a fixed number of particles, $\sum_j n_j = N$. The functional to be minimized is

$$F_v[n](N, T, U) = \mathcal{F}[n](N, T, U) + \sum_j v_j n_j, \quad (39)$$

which at the minimum will correspond to the equilibrium Helmholtz free-energy. The universal functional can be decomposed as in Eq. (17), with the same expression for the Hartree energy. The auxiliary Kohn-Sham system will have the effective potential at site j given by the v_j^{KS} in Eq. (22). After solving the noninteracting system, the site occupations have to be calculated in the canonical ensemble, which can be considerably more difficult than in the grand canonical ensemble, due to the constraint on the number of particles. More specifically, if the systems are not large enough, the chemical potential is not well defined and the Fermi-Dirac distribution cannot be used to populate the single-particle levels. For large enough systems, one could use a Fermi-Dirac distribution, setting up the chemical potential to have exactly N particles.

Making the local-density approximation to the correlation functional, Eqs. (25)–(30) can be used. After convergence of the self-consistent Kohn-Sham scheme, one can calculate the Helmholtz free-energy for the interacting system by

$$\begin{aligned} F_v(N, T, U) &= \text{Tr}\{\hat{\rho}_0[\hat{K} + k_B T \ln(\hat{\rho}_0)]\} + \sum_j \frac{U}{4} n_j^2 \\ &+ \sum_j f_c(n_j, T, U) + \sum_j v_j n_j. \end{aligned} \quad (40)$$

The first term on the right-hand side can be written in terms of the Helmholtz free-energy of the noninteracting system

$$F_0(N, T) = -k_B T \ln(Z_{0,N}),$$

$$\text{Tr}\{\hat{\rho}_0[\hat{K} + k_B T \ln(\hat{\rho}_0)]\} = F_0(N, T) - \sum_j v_j^{\text{KS}} n_j, \quad (41)$$

where $Z_{0,N}$ is the partition function of the noninteracting system with N particles. Therefore, we have

$$\begin{aligned} F_v(N, T, U) &= F_0(N, T) + \sum_j (v_j - v_j^{\text{KS}}) n_j + \sum_j \frac{U}{4} n_j^2 \\ &+ \sum_j f_c(n_j, T, U). \end{aligned} \quad (42)$$

As a final remark in this section, it should be emphasized that the density-functional approach explained above and applied to the one-dimensional inhomogeneous Hubbard model could also be applied to the model in higher dimensions. The only practical difficulty would be the absence of an exact solution for the homogeneous reference system, making the construction of a reliable local-density approximation more difficult [32–36].

IV. THE HOMOGENEOUS SYSTEM

The homogeneous 1D Hubbard model, i.e., the model in the thermodynamic limit with no external potential, can be treated exactly by the QTM method [23–25]. This approach leads to a finite set of coupled integral equations for some auxiliary functions which in turn determine the grand canonical potential per site as a function of temperature, chemical potential, and interaction strength U . By successive differentiation of the grand canonical potential with respect to these variables, all the thermodynamic quantities can be determined.

The physics of the homogeneous 1D Hubbard model at finite temperatures is well known [23–25], but in this section we will highlight aspects connected with the Helmholtz correlation energy per site [f_c in Eq. (26)], which are relevant for TBALDA and have not been discussed in the literature so far.

Considering interacting and noninteracting homogeneous systems at the same density n , we will decompose the Helmholtz correlation energy per site [Eq. (26)] to get a better understanding of its behavior. It will be written as $f_c = U_c + K_c - T s_c$, where U_c , K_c , and $-T s_c$ are its interaction, kinetic, and entropic components, respectively. The interaction component is given by the difference between the interaction energy [Eq. (3)] per site and the first-order approximation to it,

$$U_c = \lim_{L \rightarrow \infty} \frac{\text{Tr}\{\hat{\rho} \hat{U}\}}{L} - \frac{U n^2}{4} = U \left[\langle \hat{n}_{j,\uparrow} \hat{n}_{j,\downarrow} \rangle - \frac{n^2}{4} \right], \quad (43)$$

where L is the number of sites, taken to infinity in the thermodynamic limit with density n . The site j in the final expression above is arbitrary, since the system is homogeneous in the thermodynamic limit. $\langle \hat{n}_{j,\uparrow} \hat{n}_{j,\downarrow} \rangle$ represents the fraction of doubly occupied sites in the system, which will be represented by D . Therefore, $U_c = U(D - n^2/4)$. From the Helmholtz free-energy per site (f) as a function of n , T , and U , or from the grand canonical potential per site ($\omega = f - \mu n$)

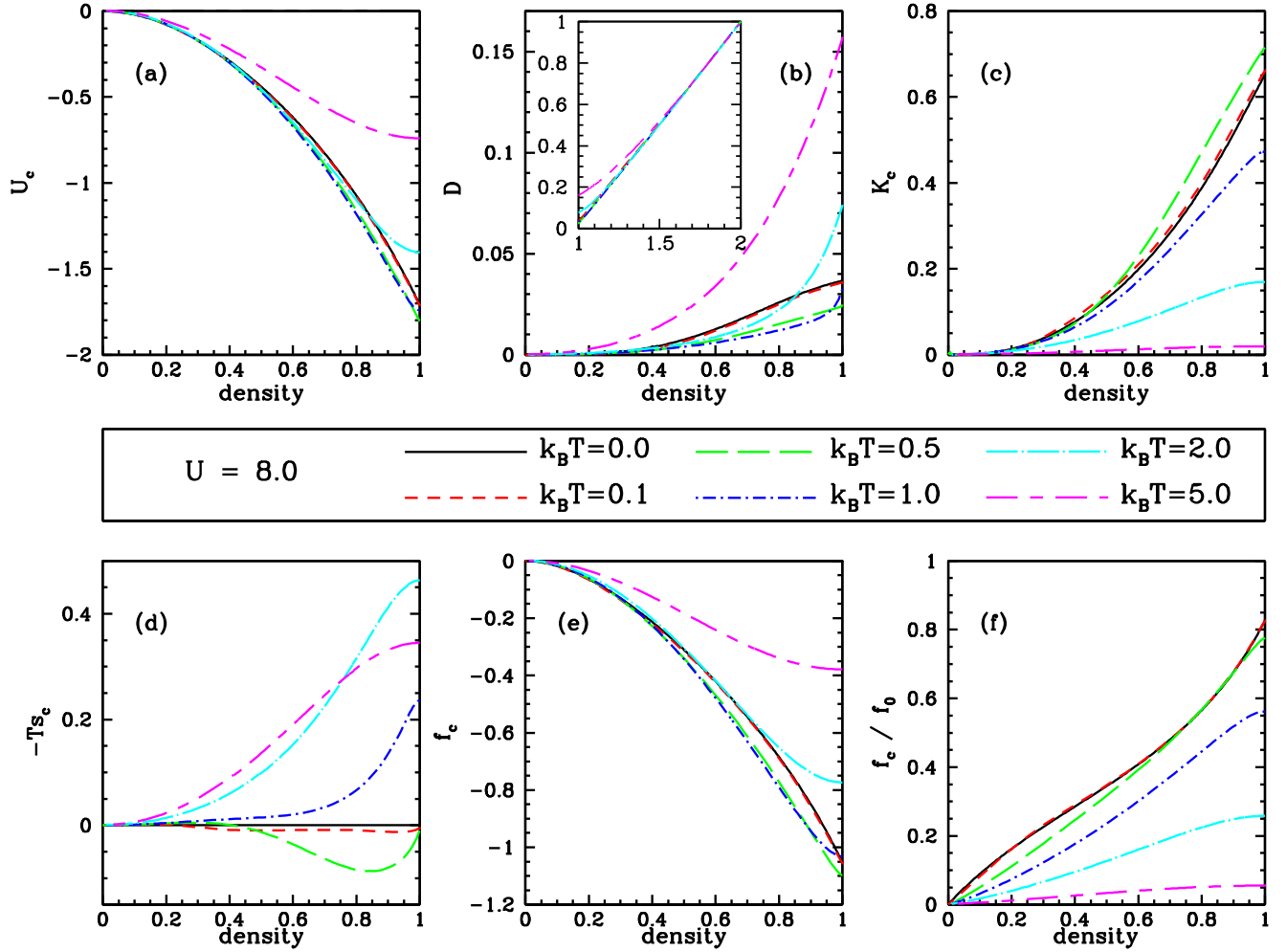


FIG. 3. (Color online) Decomposition of the Helmholtz correlation energy for $U = 8$ as a function of the density at several temperatures. Energies are in units of t . The density interval was restricted to $[0, 1]$ because the plotted functions are symmetric with respect to $n = 1$. (a) The interaction component $U_c = U(\langle \hat{n}_{j,\uparrow} \hat{n}_{j,\downarrow} \rangle - n^2/4)$. (b) The fraction of doubly occupied sites $D = \langle \hat{n}_{j,\uparrow} \hat{n}_{j,\downarrow} \rangle$. This quantity is not symmetric with respect to $n = 1$ and the inset shows its behavior for $n > 1$, when it grows fast towards 1.0 at $n = 2$, when all the sites are totally occupied. (c) The kinetic energy component K_c is the difference between the kinetic energy per site in the interacting and noninteracting models. (d) The entropic component $-Ts_c = -T(s - s_0)$, where s and s_0 are the entropies per site in the interacting and noninteracting models, respectively. (e) The Helmholtz correlation energy obtained by adding up its three components $f_c = K_c + U_c - Ts_c$. (f) Ratio between the Helmholtz correlation energy and the Helmholtz free-energy for the noninteracting system. For densities close to $n = 1$ and temperatures smaller than the gap Δ , the Helmholtz correlation energy is quite significant.

as a function of μ , T , and U , we have

$$D = \left(\frac{\partial f}{\partial U} \right)_{T,n} = \left(\frac{\partial \omega}{\partial U} \right)_{T,\mu}, \quad (44)$$

which allows us to determine the interaction component U_c . In Fig. 3(a) we show U_c as a function of the density at several temperatures for the case of $U = 8$. Exploring a particle-hole transformation, it can be shown that $U_c(n) = U_c(2 - n)$, so it is enough to consider densities from 0 to 1. The temperature dependence is weak while $k_B T < \Delta$, where Δ is the gap in the spectrum of the charge sector for $n = 1$ (when $U = 8$, $\Delta \approx 4.6795$). As can be seen in Fig. 3(b), for densities $n \leq 1$ and small temperatures, the average number of doubly occupied sites is small, making the interacting energy small and the correlation component U_c close to $-Un^2/4$. However, it is interesting to note that raising the temperature from $T = 0$,

the fraction of doubly occupied sites D initially decreases with the temperature while we still have $k_B T \ll \Delta$, and accordingly U_c also initially decreases. This is due to the fact that at small temperatures there are more spin excitations (which do not demand double occupancy) than charge excitations (which tend to increase double occupancy). This behavior has been discussed in the context of thermometry and cooling strategies for ultracold trapped atomic systems made to simulate the Hubbard model [37–42]. As the temperature becomes close to or higher than Δ/k_B , the fraction of doubly occupied sites grows, increasing U_c , whose magnitude nevertheless decreases, approaching zero as $T \rightarrow \infty$, because the correlation disappears and $\langle \hat{n}_{j,\uparrow} \hat{n}_{j,\downarrow} \rangle \rightarrow \langle \hat{n}_{i,\uparrow} \rangle \langle \hat{n}_{j,\downarrow} \rangle = n^2/4$ in this limit.

The kinetic component K_c is the difference between the kinetic energy per site in the interacting system and the kinetic energy per site in the noninteracting system. In the same way, the correlation entropy $s_c = s - s_0$ is the difference between

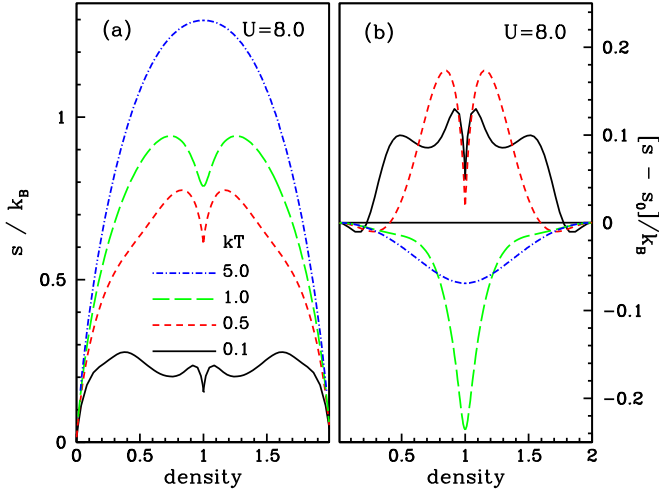


FIG. 4. (Color online) (a) Entropy per site in units of Boltzmann constant for the 1D homogeneous Hubbard model as a function of the density for $U = 8t$ and several temperatures. Energies are in units of t . By a particle-hole transformation we see that the entropy per site must be symmetric with respect to $n = 1$. For both $n = 0$ and $n = 2$ the entropy must be equal to zero. From the extrema towards half-filling, the way the entropy per site changes with the density depends strongly on the temperature. For high temperatures ($k_B T > \Delta$), the entropy is maximum at $n = 1$. For intermediate temperatures ($k_B T < \Delta$), the entropy has a local minimum at $n = 1$. At this point, the strong repulsion suppresses configurations with empty and doubly occupied sites giving rise to the local minimum of the entropy. For low temperatures, the entropy oscillates even more, but $n = 1$ is still a local minimum. (b) Difference between the entropies per site of the interacting ($U = 8t$) and noninteracting ($U = 0$) systems. For low temperatures, the interacting system has more entropy than the noninteracting one at almost all densities, while for higher temperatures we have the opposite behavior.

the entropies per site in the interacting and noninteracting systems. Since the Helmholtz free energies and entropies can be obtained from QTM equations, the kinetic component is determined from $K_c = f_c - U_c + T s_c$. In Fig. 3(c) we show K_c as a function of the density at several temperatures for the case of $U = 8$. It can be seen that $K_c > 0$ and, as U_c , it does not have a monotonic dependence with temperature. For small temperatures, K_c is an increasing function of T , but as the temperature gets close to Δ , this behavior is reversed and K_c starts to decrease. In fact, this reversion starts at temperatures significantly smaller than Δ/k_B for small densities. As $T \rightarrow \infty$, $K_c \rightarrow 0$ since correlation disappears at high temperatures.

In Fig. 3(d) we show $-T s_c$, the entropic component of the Helmholtz free-energy per site. In contrast to the other two components, the entropic one can be negative or positive (see also Fig. 4). Since $s_c = 0$ at $T = 0$, $-T s_c$ is very small at small temperatures, being initially negative. As the temperature is raised, the entropic component becomes positive and at intermediate temperatures (close to Δ/k_B) it is comparable to the kinetic component. As the temperature becomes larger compared to Δ/k_B , the correlation entropy s_c becomes smaller and smaller, which will make the product $-T s_c \rightarrow 0$ when $T \rightarrow \infty$. However, this limit is achieved much more slowly compared to the kinetic component and at high temperatures,

the entropic and interacting components can have the same order of magnitude.

The whole Helmholtz correlation energy per site is displayed in Fig. 3(e), which is similar to Fig. 3(a), since the interaction component is the most important one. On general grounds, $f_c \leq 0$ at any density and temperature. If f_0 corresponds to the Helmholtz free-energy per site for the noninteracting system with the same density as the interacting one, we have

$$f = f_0 + U \frac{n^2}{4} + f_c. \quad (45)$$

In Fig. 3(f) the ratio f_c/f_0 is displayed to better quantify how significant the contribution coming from correlation is. As expected, the precise comparison shows that correlation is specially important for densities close to 1 and temperatures lower than Δ/k_B .

In Fig. 4 the reader can see the behavior of the entropy per site [Fig. 4(a)] and of the correlation entropy per site [Fig. 4(b)] as functions of the density for the homogeneous system at several temperatures and $U = 8$.

As discussed in the previous section, to the noninteracting or Kohn-Sham auxiliary system must be applied an effective potential v^{KS} [Eqs. (21) and (22)] to keep its density equal to the density of the real interacting system. Within LDA, the correlation potential at each site (of a possibly inhomogeneous system) is given by the derivative $(\frac{\partial f_c}{\partial n})_{T,U}$ evaluated at the site occupation, so some familiarity with the density dependence of $v_c = (\frac{\partial f_c}{\partial n})_{T,U}$ is helpful to understand the behavior of the Kohn-Sham system.

From the QTM equations, we can get the density as a function of the chemical potential and the inverse of this function allows us to determine the correlation potential as indicated in Eq. (29). As displayed in Fig. 5(a), at $T = 0$ the correlation potential is discontinuous at $n = 1$. The jump is equal to the gap Δ [14,28]. It is interesting to note that this gap is entirely due to correlation, since there is no gap in the Kohn-Sham spectrum of single-particle energies for a half-filled homogeneous system. For finite temperatures, the discontinuity disappears, but v_c changes fast around $n = 1$ if $k_B T \ll \Delta$. As the temperature is raised, the function v_c becomes smoother, converging uniformly to zero in the limit $T \rightarrow \infty$. An abrupt change of the correlation potential around the density $n = 1$ may sometimes make the convergence of the Kohn-Sham self-consistent loop very slow. This point has been discussed recently in Ref. [16] and a possible solution has been proposed in Ref. [43].

Figure 5(b) illustrates the behavior of v_c for several values of interaction strength U at the same temperature $k_B T = 0.5$. For large U we have $k_B T \ll \Delta$, making v_c be almost discontinuous at $n = 1$. As U decreases, so does Δ , and the correlation potential becomes smoother and smoother. For $U = 0$ we would naturally have $v_c = 0$ at any density.

V. COMPARISON WITH EXACT DIAGONALIZATION IN A SHORT CHAIN

The formalism developed in Sec. II can be used for any kind of external potential. Before testing the performance of TBALDA, it is important to explain how TBALDA was

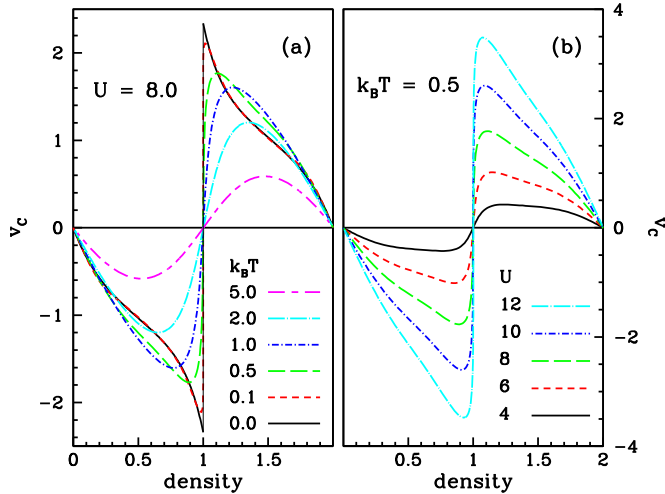


FIG. 5. (Color online) (a) Correlation potential ($v_c = df_c/dn$) as a function of density for $U = 8$ and several temperatures. Energies are in units of t . At $T = 0$, the correlation potential has a discontinuity at $n = 1$ with a jump equal to the gap energy (Δ). At finite temperatures, the discontinuity disappears. However, v_c will change rapidly around $n = 1$ while $k_B T \ll \Delta$. (b) Correlation potential for $k_B T = 0.5$ for several interaction strengths. As U increases, the gap energy also increases, and the change of the correlation potential around $n = 1$ becomes more pronounced.

actually implemented. In this work, for given values of U , temperature, and chemical potential, we solve the QTM equations for the homogeneous model to find the density, the correlation Helmholtz free-energy per site, as well as its derivative with respect to the density (correlation potential) and the correlation entropy per site. Repeating the calculation for several values of chemical potential, we generate a fine mesh of densities in the interval $[0, 2]$. Let us call this whole computation a mesh computation. For densities not presented in the mesh, a careful numerical interpolation is used to extract the quantities of interest keeping accuracy. Each mesh computation takes a few hours in a 2.4 GHz desktop computer. Given U and $k_B T$, after the mesh computation, we can study within LDA the inhomogeneous Hubbard model for arbitrary external potential. However, for fixed external potential, the study of its properties as a function of temperature, requires a mesh computation for each temperature. It would be easier if we had accurate analytical fittings to the dependence on temperature and U of the thermodynamic data from QTM equations. An important first step in this direction has been given in Ref. [16], where an analytical parametrization is proposed to the correlation free-energy that allows an accurate description of the correlation potential. However, the resulting temperature dependence of the entropy per site is not accurate for $k_B T < 1$ [44], so that we had to follow the more time demanding approach of doing a mesh computation for each temperature and U to avoid introducing spurious errors in the method. While density profiles computed using the parametrization will be accurate [44], thermodynamic properties, specially the entropy, computed using the parametrization, can have significant errors.

In this section we consider a nine-site Hubbard chain with $U = 4.0$, submitted to the harmonic external potential

$V_j = (j/2)^2$, $-4 \leq j \leq 4$, with open boundary condition. The thermodynamic properties of this inhomogeneous system were calculated from numerical exact diagonalization leading all eigenvalues and eigenvectors. Exploring conservation of number of particles and of spin angular momentum (S^2 and S_z), the exact diagonalization is carried out in a few hours using a 2.4 GHz desktop computer. Since the number of eigenvalues grows exponentially with the chain size, going beyond nine sites would demand considerably greater computational resources than used here. Nine sites are already close to the maximum one could achieve computing all eigenvalues and eigenvectors, so it is a size neither too big, making exact calculations possible, nor too small, making the LDA applicable.

Having exact results, we can test the performance of TBALDA. A test with a small chain is a tough one because finite size effects and the spectrum discreteness are significant and cannot be properly described by a local-density approximation based on results for the homogeneous system in the thermodynamic limit. Since a local-density approximation is better for smooth external potentials, if TBALDA performs relatively well in this test, we will have a strong indication that it will perform well enough in the large systems we are ultimately interested in. A comparison for larger systems with around 100 sites is provided in the end of the section, where density profiles obtained from TBALDA are compared with density profiles obtained from DMRG calculations in Ref. [46] and excellent agreement is observed.

We analyzed the grand canonical potential, the entropy, the number of particles, and the site densities in broad ranges of temperature and chemical potential. Once we have the density at the end of the self-consistent Kohn-Sham cycle, the number of particles is trivially computed. The grand canonical potential is computed using Eq. (34) and the entropy comes from Eq. (37). From the extensive comparison between BALDA and QMC or DMRG results at $T = 0$ [30,45], that usually indicates small errors in the ground-state energy and site occupations, we could expect small errors in the grand canonical potential, site occupations, and number of particles at finite temperatures and it is exactly what we have found. Table I summarizes the error

TABLE I. Error analysis of TBALDA results for a nine-site chain with external potential $V(j) = j^2/4$, $-4 \leq j \leq 4$, and an open boundary condition. We made comparisons for 120 values of chemical potential in the interval $[-1, 5]$ at three representative temperatures. We show average absolute relative error/maximum absolute relative error (percent values) for the grand canonical potential (Ω), number of particles (N), entropy (S), and site occupations (n_j).

	Av. rel. error (%) / Max. rel. error (%)		
	$k_B T = 1.0$	$k_B T = 0.5$	$k_B T = 0.2$
Ω	0.12/0.33	0.28/0.72	0.63/2.8
N	0.38/3.3	0.46/1.7	1.7/4.9
S	0.94/5.8	1.5/7.4	8.4/31
n_0	0.64/4.6	0.49/3.3	1.5/5.1
n_1	0.74/5.2	0.68/3.0	1.6/5.0
n_2	0.94/6.5	1.2/5.6	2.8/7.5
n_3	1.1/6.5	2.2/5.2	6.2/16
n_4	1.6/5.8	5.6/12	15/45

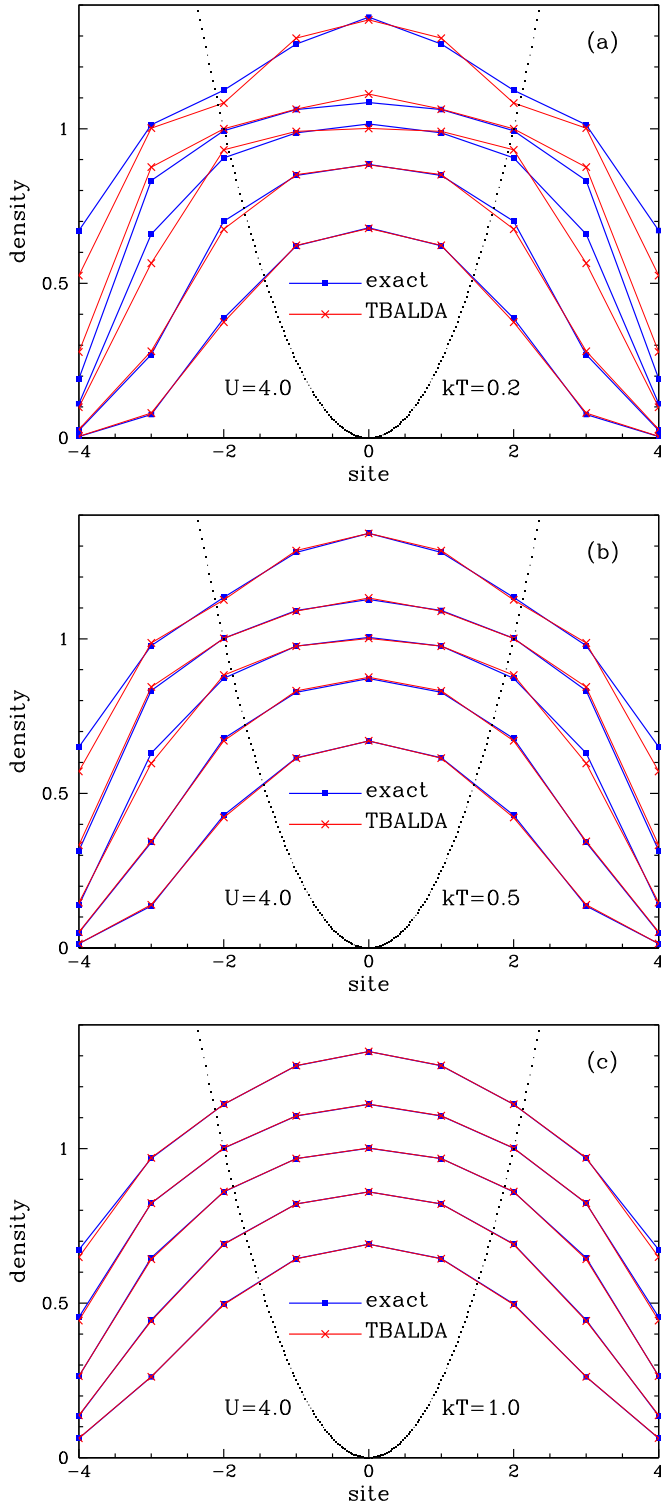


FIG. 6. (Color online) Density profiles from exact diagonalization and from the Kohn-Sham scheme using TBALDA. At each panel we show data for chemical potential equal to 0, 1, 2, 3, and 4. The dotted line represents the confining potential $V(j) = j^2/4$.

analysis found in this comparison. Figure 6 displays density profiles obtained by both exact diagonalization and the DFT-TBALDA approach. We plotted density profiles for situations very close to those with the largest errors found while varying

the chemical potential in broad intervals (see Table I). Despite the smallness of the system, the agreement is quite well.

Two main features are clear. First, the errors decrease as the temperature increases. This can be understood from the fact that the correlation becomes less important at higher temperatures, as discussed in Sec. IV and also because a small temperature can be smaller than the typical energy level separation (ΔE). In this situation we do not expect TBALDA works well. For the present small system we have $\Delta E \approx 0.5$ and even when $k_B T = 0.2$ we have reasonable accuracy. Second, the errors become more significant as we move to the ending sites. There are two reasons for this behavior. One is elementary: the densities in the ending sites are smaller due to the confining potential, so the relative errors there are expected to be larger than in the central sites. The other reason is more fundamental: we have a chain with an open boundary condition and our approach based on TBALDA simply cannot deal appropriately with this situation where the last sites have just one neighbor. With this in mind, the performance of TBALDA is in fact surprisingly good in the last sites of the chain for the vast majority of the studied cases.

In spite of the smallness of the system and some difficulty to reproduce the densities in the last sites, TBALDA results for extensive quantities (namely, grand canonical potential, number of particles, and entropy) are quite accurate as can be seen in Table I. The entropy typically gives rise to a small contribution to the grand canonical potential (through the $-TS$ term) and its determination requires an accurate description of the temperature dependence of the grand canonical potential. The derivative of our approximate grand canonical potential functional with respect to the temperature at its minimum is given by Eq. (37), being unnecessary to make numerical derivatives to compute the TBALDA approximation to the entropy.

We conclude that TBALDA has been successful in this tough test of a small chain. For a parabolic confining potential given by $V(x) = (x/L)^2$, if we consider that (i) TBALDA is exact by construction in the limit $L \rightarrow \infty$ (homogeneous system) and (ii) it is already quite accurate for the case of $L = 2$ in a short chain with an open boundary condition; given the nature of a local-density approximation, one can only expect accurate results from TBALDA for intermediate values of L , increasing accuracy for larger values of L . It should also be noted that the role of correlation decreases as we increase the temperature as discussed in the previous section. At $T = 0$ BALDA has typical accuracy of few percent [14,16,30,45] in the ground-state energy and site occupations. At large temperatures, the DFT approach will be certainly successful because the local-density approximation will be done for a small quantity (correlation energy) and the system behavior will be close to the behavior of the noninteracting Kohn-Sham system. Accordingly, for intermediate temperatures we expect accuracy of a few percent. The only limitation of accuracy occurs when $0 < k_B T < \Delta E$, where ΔE is the typical energy level separation in the confined system, that is of order $1/L$. For $L \approx 100$ this lowest temperature is much slower than the temperatures achieved in experiments [18].

Therefore, one can treat larger systems, where the external potentials are smooth ($L \gg 2$), expecting that thermodynamic properties be accurately determined. This expectation is

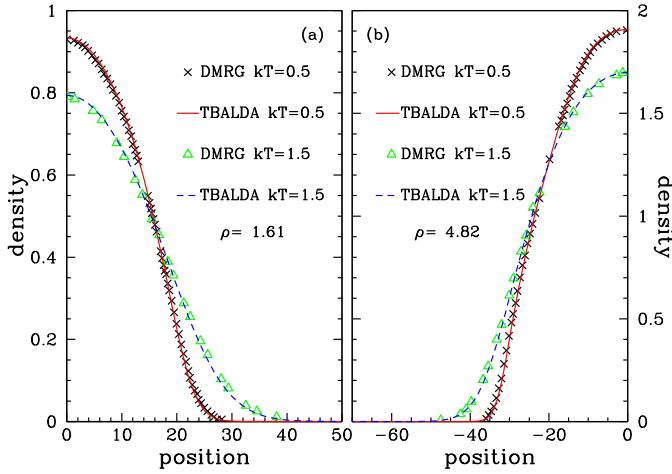


FIG. 7. (Color online) Density profiles for the 1D harmonically confined Hubbard model with $U = 1.44$ and confining potential $V(x) = (x/L)^2$. Comparison between TBALDA results and DMRG results extracted from Figs. 9(b) and 10(b) of Ref. [46]. In this figure $\rho = N/(\sqrt{2}L)$ represents the rescaled density as defined in Ref. [46].

confirmed for the case of density profiles in Fig. 7, where we compare density profiles obtained by TBALDA with density profiles obtained by DMRG calculations at finite temperature from Ref. [46]. Excellent agreement between both techniques is observed.

VI. THERMODYNAMICS OF THE HARMONICALLY CONFINED ONE-DIMENSIONAL HUBBARD MODEL

A. General aspects

In this section we consider the case of harmonic traps, whose external potential has the general form

$$v_j = (j/L)^2. \quad (46)$$

Accordingly, $2L$ can be considered the typical size of the confined system. In what follows it will be helpful to refer to this size ($2L$) as the volume (V) of the system. Given the general familiarity with classical thermodynamics, this abuse of notation will make our treatment more appealing. Figure 8 displays typical density profiles and makes clear that in a harmonically confined system the number of particles outside its volume $2L$ can be quite significant. In spite of this fact and of the characteristic inhomogeneity of the system, we show below that its global thermodynamic description can be done in a way totally similar to the classical thermodynamics of homogeneous systems.

Consider the behavior of usually extensive quantities, like internal energy, free-energy, entropy, and number of particles of usual systems with sharp boundaries as we increase the volume keeping temperature and chemical potential fixed. In the thermodynamic limit, when surface effects become negligible, any extensive quantity is proportional to the volume. Figure 9 illustrates what happens for the inhomogeneous harmonically confined Hubbard model. The linear dependence of the grand canonical potential (and any other extensive property) on the volume is observed even for relatively small volumes, opening

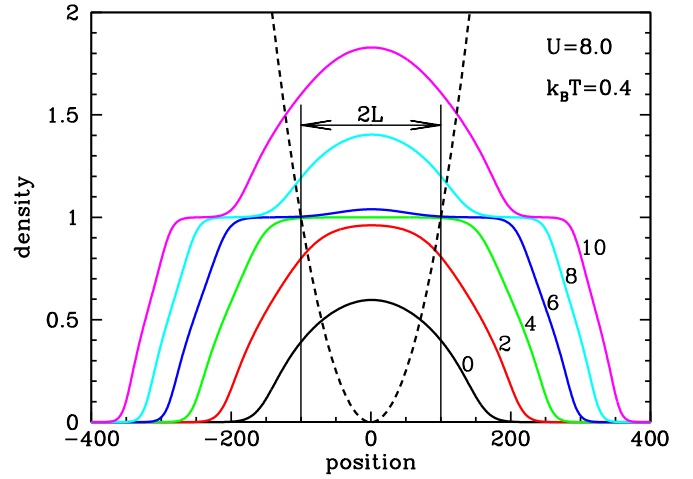


FIG. 8. (Color online) Density profiles for system “volume” $2L = 200$, $U = 8.0$, and $k_B T = 0.4$ for different values of the chemical potential ($\mu = 0, 2, 4, 6, 8$, and 10). The dashed line represents the parabolic potential $V(x) = (x/100)^2$. As the chemical potential increases, a significant fraction of the particles will be found outside the interval $[-L, L]$. As the temperature is much smaller than the gap ($k_B T/\Delta \approx 0.085$), the central plateau around density equal to 1.0 is visible for $\mu = 4$, as well as lateral plateaus are also visible for larger values of the chemical potential. Energies are in units of t .

the possibility for a classical thermodynamic treatment of this system.

The fact that a harmonically confined system has no surface, with the external potential growing slowly, suggests that the finite-size correction to the thermodynamic limit of the ratio

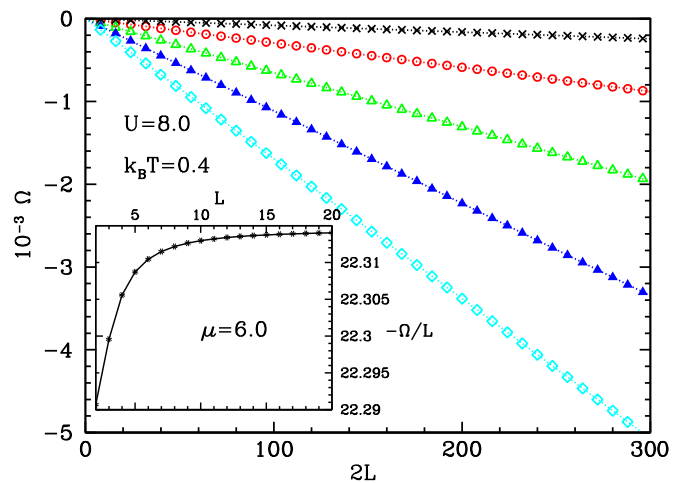


FIG. 9. (Color online) Grand canonical potential (Ω) as a function of the volume ($V = 2L$) at $k_B T = 0.4$ for different values of the chemical potential. Energies are in units of t . From top to bottom we have $\mu = 0, 2, 4, 6$, and 8 . The linear behavior since small sizes is clear from the excellent distribution of the points over the linear fittings to them (dotted lines). This picture is only illustrative of this fact which was observed for all temperatures, chemical potentials, and interaction strengths in broad ranges investigated. Inset: Deviation from the linear behavior for small L , showing that the thermodynamic limit is achieved fast.

between any extensive quantity and the volume $2L$ can be special. In fact, for the case of the ground-state energy, it was found [47] that $E/(2L) = \epsilon_\infty + 1/(2L/\xi)^\gamma$, with the exponent $\gamma > 1$ (around 1.4 for $U = 2.0$). This exponent larger than the common value of 1 makes the thermodynamic limit ϵ_∞ rapidly achievable and explains the results also found for finite temperatures in Fig. 9.

Having the chemical potential, the temperature, the interaction strength (U), and the volume as independent variables, the grand canonical potential $\Omega(\mu, T, U, V)$ will give the complete thermodynamic description of the system. In particular, we have

$$d\Omega = -SdT - Nd\mu + N_D dU - p dV, \quad (47)$$

where S is the entropy, N is the number of particles, N_D is the number of doubly occupied sites, and p is the pressure. But what does the pressure mean in this harmonically confined Hubbard model? To answer this, it is enough to work out from Eq. (6) relating the grand canonical potential to the grand partition function $Z_G = \text{Tr}\{e^{\beta(\hat{H} - \mu\hat{N})}\}$. We have

$$\begin{aligned} \left(\frac{\partial\Omega}{\partial V}\right)_{\mu,T,U} &= \frac{1}{Z_G} \sum_R \frac{\partial}{\partial V} (E_R - \mu N_R) e^{-\beta(E_R - \mu N_R)} \\ &= \frac{1}{Z_G} \sum_R \frac{\partial}{\partial V} \langle R | \hat{H} - \mu \hat{N} | R \rangle e^{-\beta(E_R - \mu N_R)} \\ &= \frac{1}{Z_G} \sum_R \langle R | \frac{\partial \hat{H}}{\partial V} | R \rangle e^{-\beta(E_R - \mu N_R)} = -\frac{\langle \hat{V}_{\text{ext}} \rangle}{L}. \end{aligned} \quad (48)$$

where $\hat{V}_{\text{ext}} = \sum_j (\frac{j}{L})^2 \hat{n}_j$ is the external potential operator due to the harmonic trap. Therefore, the trap pressure is given by

$$p = \frac{\langle \hat{V}_{\text{ext}} \rangle}{L} = \frac{2\langle \hat{V}_{\text{ext}} \rangle}{V}. \quad (49)$$

The proportionality between Ω and volume in the harmonically confined system seen in Fig. 9 can be mathematically expressed by

$$\Omega(\mu, T, U, \lambda V) = \lambda \Omega(\mu, T, U, V) \quad (50)$$

for real λ . This immediately gives us the familiar Euler relation

$$\Omega(\mu, T, U, V) = -p(\mu, T, U)V, \quad (51)$$

where the trap pressure is a function of temperature, chemical potential, and U only.

Any other thermodynamic function can be computed from derivatives of $p(\mu, T, U)$. In particular, the first derivatives give the particle number, the entropy, and the number of doubly occupied sites,

$$N(\mu, T, U, V) = \left(\frac{\partial p}{\partial \mu}\right)_{T,U} V, \quad (52)$$

$$S(\mu, T, U, V) = \left(\frac{\partial p}{\partial T}\right)_{\mu,U} V, \quad (53)$$

$$N_D(\mu, T, U, V) = -\left(\frac{\partial p}{\partial U}\right)_{\mu,T} V, \quad (54)$$

so

$$dp = \frac{N}{V} d\mu + \frac{S}{V} dT - \frac{N_D}{V} dU, \quad (55)$$

that is the Gibbs-Duhem relation between the differentials of the four intrinsically intensive quantities for this kind of thermodynamic system. In the following we will assume U is kept constant during the thermodynamic transformation and will omit this variable for simplicity. In the next subsection we will discuss how U affects the behavior of the system under isentropic expansion, as well as consider isentropic changes of this parameter.

Let us introduce some thermodynamic coefficients obtained from the second derivatives of the trap pressure. We have the isothermal charge susceptibility

$$\chi_t = \frac{1}{N} \left(\frac{\partial N}{\partial \mu}\right)_{T,V} = \frac{V}{N} \left(\frac{\partial^2 p}{\partial \mu^2}\right)_T, \quad (56)$$

the specific heat at constant μ and V ,

$$c_{\mu,v} = \frac{T}{N} \left(\frac{\partial S}{\partial T}\right)_{\mu,v} = \frac{TV}{N} \left(\frac{\partial^2 p}{\partial T^2}\right)_\mu, \quad (57)$$

and the thermal particle-increment coefficient

$$v = \frac{1}{N} \left(\frac{\partial N}{\partial T}\right)_{\mu,v} = \frac{V}{N} \frac{\partial^2 p}{\partial T \partial \mu}. \quad (58)$$

Note the Maxwell relation $(\frac{\partial S}{\partial \mu})_{T,V} = (\frac{\partial N}{\partial T})_{\mu,v} = vN$. While χ_t and $c_{\mu,v}$ are never negative as a consequence of the second law of thermodynamics, the thermal particle-increment coefficient can assume positive and negative values.

With the above definitions we can write

$$dp = \frac{s}{v} dT + \frac{1}{v} d\mu, \quad (59)$$

$$dN = vNdT + \chi_t Nd\mu + \frac{1}{v} dV, \quad (60)$$

$$dS = \frac{c_{\mu,v}}{T} NdT + vNd\mu + \frac{s}{v} dV, \quad (61)$$

where $s = S/N$ is the entropy per particle and $v = V/N$ is the volume per particle. From the differentials in Eqs. (59)–(61), any other thermodynamic coefficient can be written in terms of χ_t , $c_{\mu,v}$, and v . Some of them are listed in Table II.

TABLE II. Common thermodynamic coefficients and their relation to those defined in Eqs. (56) and (57).

Adiabatic charge susceptibility	$\chi_s = \frac{1}{N} \left(\frac{\partial N}{\partial \mu}\right)_{S,V} = \chi_t - \frac{v^2 T}{c_{\mu,v}}$
Thermal expansion coefficient	$\alpha = \frac{1}{V} \left(\frac{\partial V}{\partial T}\right)_{p,N} = s\chi_t - v$
Specific heat at constant volume	$c_v = \frac{T}{N} \left(\frac{\partial S}{\partial T}\right)_{V,N} = c_{\mu,v} - \frac{v^2 T}{\chi_t}$
Specific heat at constant pressure	$c_p = \frac{T}{N} \left(\frac{\partial S}{\partial T}\right)_{p,N} = c_{\mu,v} + Ts(s\chi_t - 2v)$
Isothermal compressibility	$\kappa_t = -\frac{1}{V} \left(\frac{\partial V}{\partial p}\right)_{T,N} = v\chi_t$
Adiabatic compressibility	$\kappa_s = -\frac{1}{V} \left(\frac{\partial V}{\partial p}\right)_{S,N} = \frac{c_{\mu,v}}{c_p} v\chi_s = \frac{c_v}{c_p} \kappa_t$

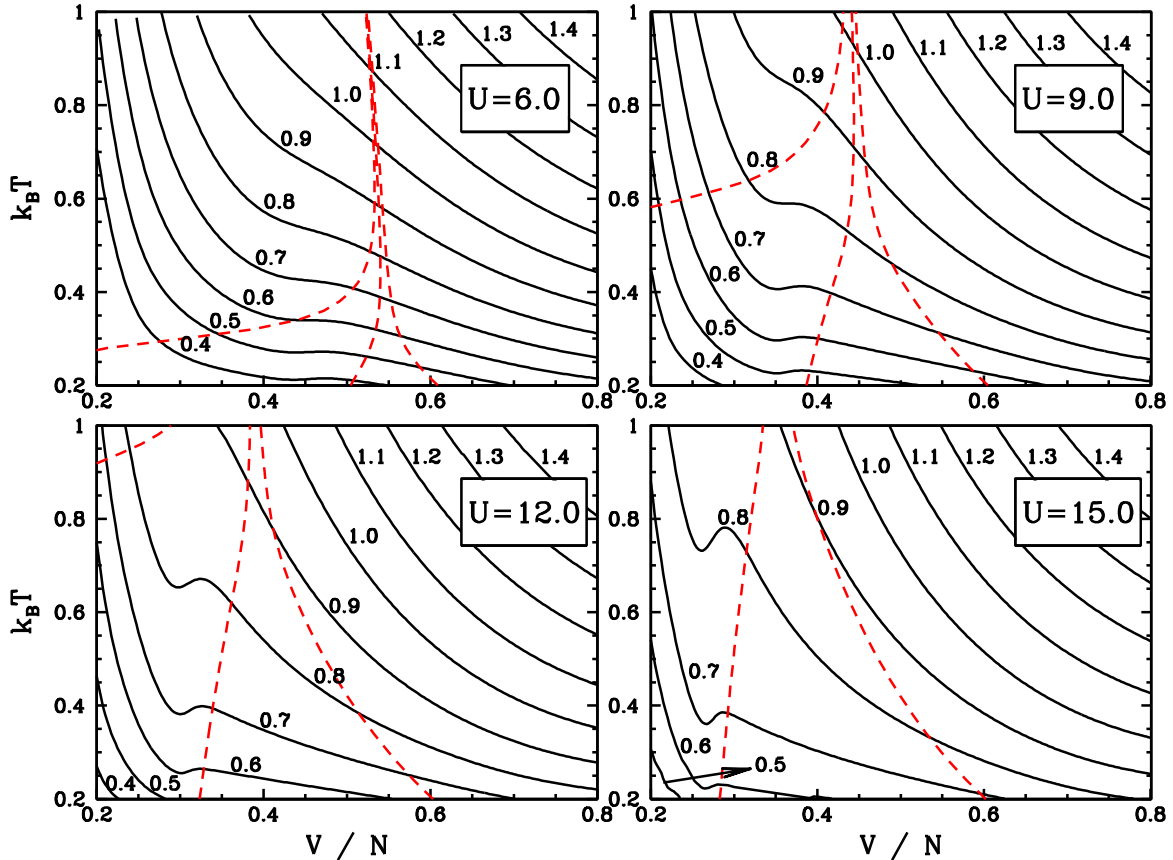


FIG. 10. (Color online) Temperature dependence on volume per particle during isentropic transformations of harmonically trapped systems. We have results for four different values of U . For each U we display curves for several values of entropy per particle in units of Boltzmann constant. The region below the rightmost and leftmost dashed lines corresponds to the locus on TV plane where the trapped systems present a plateau in their density profiles whose size is at least 10% of the volume ($2L$). Due to the finite temperature, the density n is not perfectly constant in the plateau. We have adopted the criteria of considering a site i as part of the plateau if $|n_i - 1.0| < 10^{-3}$. On the right of the central dashed line, the plateau is central, while on the left, it is lateral. For small values of entropy per particle, there are narrow ranges of specific volumes where the temperature increases during the isentropic expansion. This anomalous behavior becomes more evident as U is increased.

B. Isentropic transformations

If the parabolic external potential has its curvature slowly changed to allow thermodynamic equilibrium, we have a thermodynamic transformation with constant particle number (for negligible loss of particles) and constant entropy (there is no heat transfer). The change in curvature represents a change in the volume ($2L$) as defined above.

Figure 10 displays, for four different values of U , how the temperature depends on the volume per particle during isentropic transformations at several values of entropy per particle. The usual adiabatic cooling under expansion is observed almost everywhere. However, for low enough specific entropy, we observe temperature increase during expansion in narrow intervals of specific volume. The anomalous behavior becomes stronger as the parameter U increases. Such behavior is unusual but it is thermodynamically allowable because

$$\left(\frac{\partial T}{\partial v}\right)_s = -\frac{\alpha T}{c_v \kappa_t}, \quad (62)$$

and the thermal expansion coefficient (α) can be negative (as it happens, for example, with water below 4°C at 1 atm).

At constant particle number and entropy, the volume of the trap will determine the temperature of the confined system, except in the small region where the temperature is not monotonic.

The behavior of the thermodynamic properties is naturally related to the density profile, in fact, as discussed in Sec. II, the density profile determines the thermodynamics of the system. In each panel of Fig. 10 the area below the leftmost dashed line and the rightmost dashed line is the region where the system density profile presents a plateau with half-filled sites, where the system behaves locally as a Mott insulator, presenting very low compressibility. On the right of the central dashed line, the plateau is in the middle of the trap. Compressing the system, the central plateau will increase, the density remains constant due to the energy gap preventing double occupation in the middle of the trap. Continuing the compression, there will be a point where it starts to be energetically favorable to increase the density in the center of the trap instead of increasing the plateau extension. The density profiles start to have lateral plateaus separated by a bump where the density is larger than one. The central dashed line in the panels of Fig. 10 locates the transition: central plateaus on the right and lateral plateaus on the left.

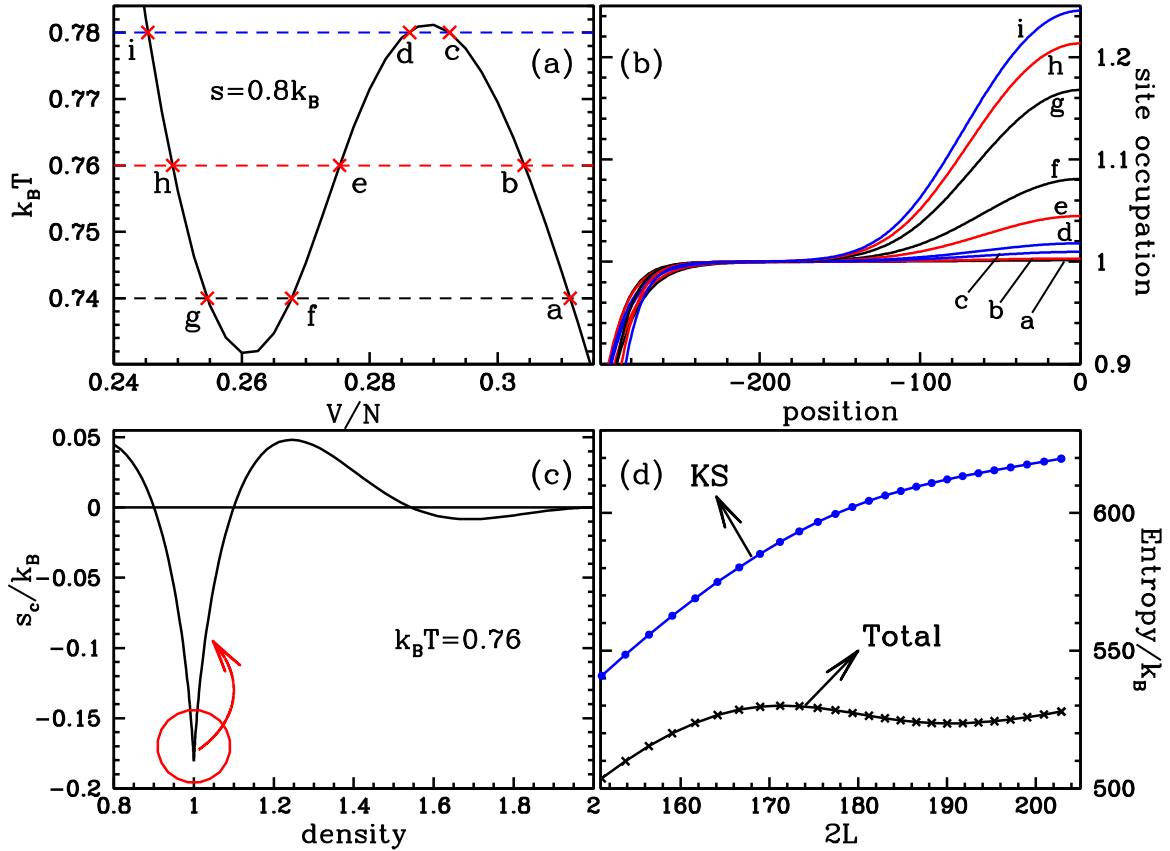


FIG. 11. (Color online) Cartoon to explain the anomalous change of temperature in isentropic transformation. In (a) we zoom the isentropic line with entropy per particle $s = 0.8k_B$ from the $U = 15$ panel of Fig. 10. We show three isothermal lines crossing the isentropic line at three different points. For each crossing, the corresponding density profile is displayed in (b). The correlation entropy per site of the homogeneous model with $k_B T = 0.76$ is displayed as a function of the density in (c). Its pronounced minimum at half-filling is noticeable (see also Fig. 4). (d) The total entropy and the Kohn-Sham entropy as functions of the volume ($2L$) for $k_B T = 0.76$. As the system is compressed ($b \rightarrow e \rightarrow h$), the rate of increase of the correlation entropy due to the increase of the density in the center of trap can compensate the decrease of the KS entropy, making the total entropy increase in some range of volumes.

Due to the finite temperature, the density is not strictly equal to one, but for $k_B T$ smaller enough than the energy gap, the density variation around one will be negligible. The criteria used to draw the dashed lines in Fig. 10 was to have at least $0.2L$ sites with densities n_i satisfying $|n_i - 1| < 10^{-3}$.

Starting with a given number of particles and a weakly confined system, we can get the insulating phase in the center of the trap by decreasing its volume only if the entropy per particle is low enough. Consider, for example, the case $U = 9$. We would need $s < 0.9 k_B$ to have a reasonable range of system volumes presenting flat plateaus. For higher values of the entropy per particle, when the volume per particle becomes close to 0.5, the temperature of the system will be already high enough to prevent the formation of a flat plateau in the density profile.

To discuss the influence of the interaction U on the isentropic curves of Fig. 10, we have to take into account that the temperature must be compared to the energy gap (Δ), which is an increasing function of U . The formation of plateaus in the density profiles, i.e., the appearance of Mott insulator regions in the trapped system, has direct influence on the thermodynamics properties. The formation of plateaus depends on the ratio $k_B T/\Delta$, therefore some degree of scaling

with Δ in the temperature axis should be expected and, in fact, it is clear in Fig. 10 that, increasing U , the anomalous behavior is observed to shift to higher temperatures as well as the dashed lines, that delimit the plateau regions in the TV plane, have their temperatures scaled by the gap Δ .

It is also interesting to observe that the unusual behavior shifts to smaller specific volumes as U increases. Since the unusual behavior happens in the lateral plateau region, the shift to smaller specific volumes is a consequence of the fact that, starting from a central plateau, we need to compress the system until the potential energy due to the trap potential at the borders of the plateau becomes comparable to the gap Δ to start observing lateral plateaus. Therefore, larger U , the higher the required compression.

The unusual temperature increase under isentropic expansion can be understood if we analyze the changes in the density profile during the thermodynamic transformation and take into account the very characteristic dependence of the correlation entropy on density for the one-dimensional Hubbard model. Figure 11 illustrates the situation for the case $U = 15$. Consider the change of the density profile during a compression (we prefer to make the argument for a compression instead an expansion). The bump in the center

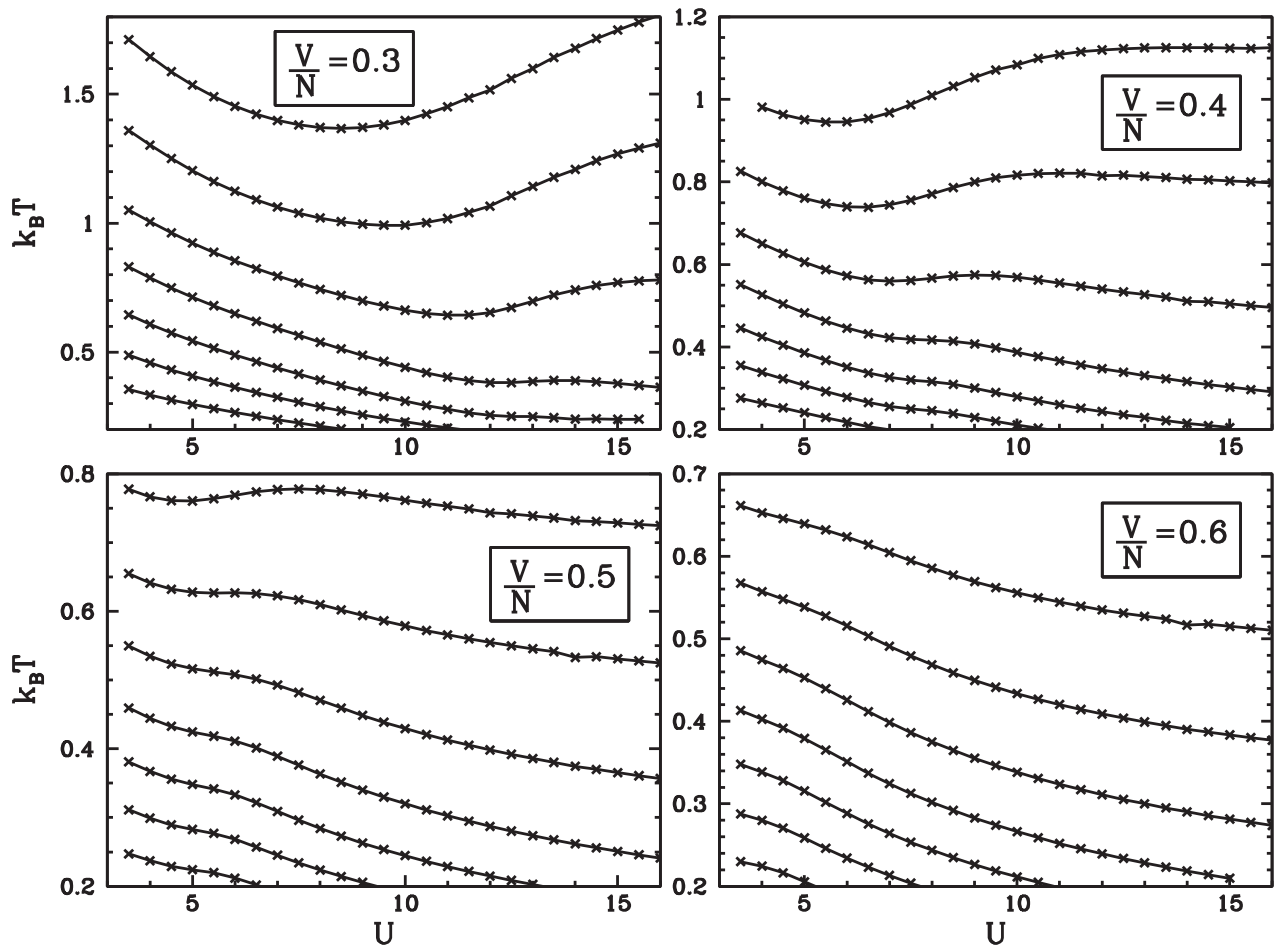


FIG. 12. Temperature dependence on the interaction strength U with entropy, volume, and number of particles kept constant. Each panel corresponds to a different volume per particle. Each curve corresponds to a different entropy per particle. From bottom to top we have $S/Nk_B = 0.4, 0.5, 0.6, 0.7, 0.8, 0.9$, and 1.0 in all panels.

of the trap grows in height and width and the borders of the lateral plateaus move inwards to keep the number of particles constant. The number of sites with density larger than one increases and the lateral plateaus shrink.

Suppose for a moment that the temperature is constant. We decompose the total entropy as the sum of Kohn-Sham entropy and correlation entropy [see Eq. (37)]. Given the sharp minimum of the correlation entropy per site at $n = 1$ [Fig. 11(c)], the correlation entropy (computed by LDA) increases when some sites have their occupations increased from $n = 1$ to $n \gtrsim 1$. Eventually such increase can overcome the decrease of the Kohn-Sham entropy (for a noninteracting system, the entropy always decreases under isothermal compression), leading to an increasing total entropy. To restore the entropy, we need to lower the temperature, so we get the unusual temperature decrease under isentropic compression.

Under further compression, the sites in the center of the trap will assume densities with values about the local maximum of the correlation entropy. Accordingly, the increasing rate of the correlation entropy will fall. At some point the increase of the correlation entropy will cease compensating the decrease of the Kohn-Sham entropy and the temperature change under isentropic transformation gets back to the usual behavior. It is interesting to point out that the unusual increase of temperature

in isentropic expansion may be a feature displayed only by the one-dimensional system. Similar plots of the temperature as a function of the average density ($N/2L$) for the repulsive two-dimensional Hubbard model under parabolic confinement were reported in Ref. [38] without presenting such unusual behavior. However, it cannot be discarded that the average densities investigated in that reference may be too high to allow the observation of the unusual behavior.

If we look carefully at Fig. 10 we will observe that the isentropic curves with $S/N = 0.8k_B$ and $S/N = 0.7k_B$ around $V/N = 0.3$ seem to repel each other as U increases. This behavior suggests to be valid to study how temperature changes as U is increased isentropically at constant volume. Figure 12 illustrates the situation. Before discussing it, it is helpful to analyze the dependence on U of the entropy per site in the homogeneous model.

In the homogeneous model the entropy will depend significantly on U if the density is close to 1 and will have negligible dependence on U if the density is far from 1, since at low densities of particles or holes, the interaction is less important. The scenario is illustrated in Figs. 13(a), 13(b), and 13(c). The temperature has to be taken into account in this discussion. First, consider the case of a small temperature (compared to typical values of the gap Δ). As U increases, for densities

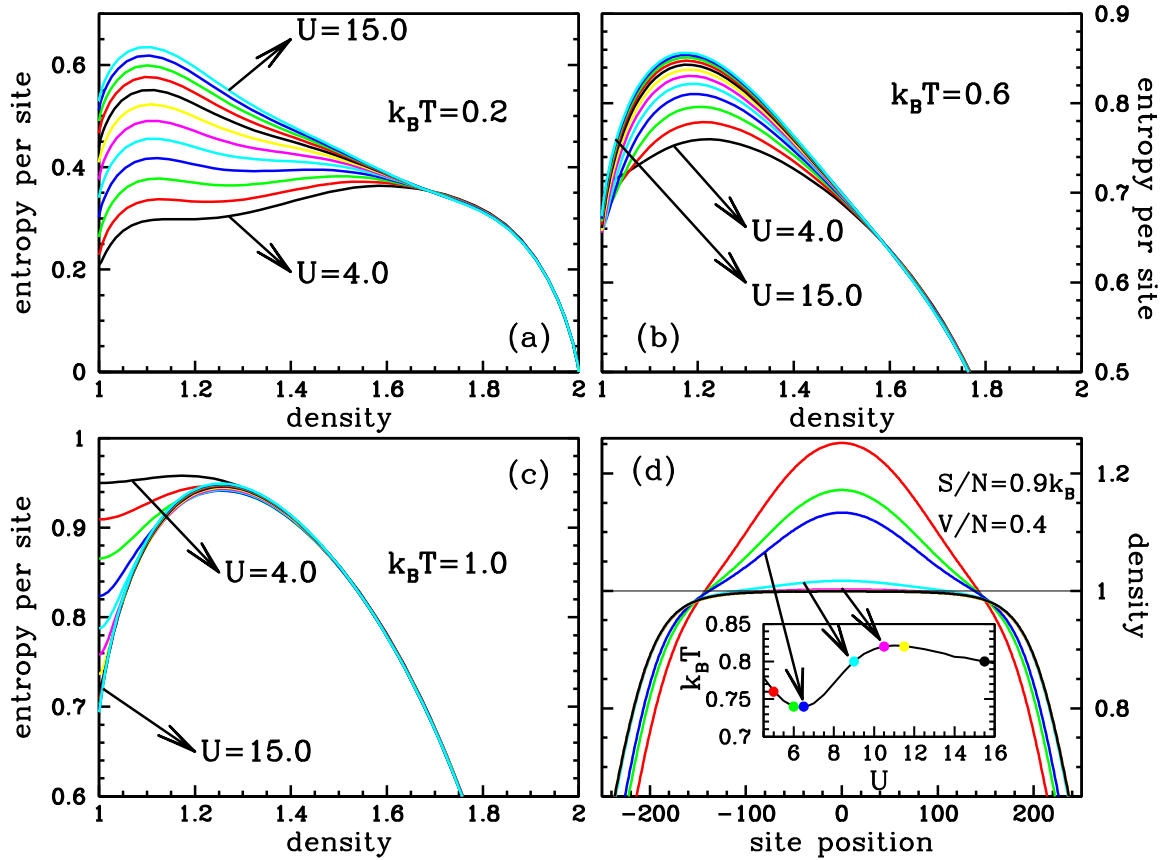


FIG. 13. (Color online) (a) Entropy per site as a function of the density in the homogeneous Hubbard model for $U = 4, 5, \dots, 15$ at $k_B T = 0.2$. (b) and (c) Same as (a) but for $k_B T = 0.6$ and $k_B T = 1.0$, respectively. As the entropy is symmetric around half-filling, we only show results for density greater than 1. It is strikingly that beyond some density, the dependence on U becomes essentially negligible. Very close to half-filling the entropy is not monotonic as a function of U and this behavior becomes more pronounced as the temperature is increased. (d) Correlation between the change of the density profile of the confined system and the change of the temperature when the intrasite interaction U changes isentropically, highlighting the range of U where the temperature rises as U increases. Data are for a system with $S/N = 0.9k_B$ and $V/N = 0.4$.

around half-filling, the entropy per site increases. This can be understood from the fact that most of the excitations present in the system are in the spin sector [46,48]. Those excitations have energies dispersed over a width of order $J = 4t^2/U$. As U is increased, J decreases, more excitations are present for the same temperature, and the entropy increases accordingly. For a higher temperature, the range of densities where the entropy changes with U shrinks. If the temperature is high enough to allow charge excitations for small U s, as U increases the number of such charge excitations will decrease fast, the number of spin excitations will increase, and the entropy per site typically will increase, but for densities very close to one, the entropy per site can in fact decrease while U is not too large. Increasing the temperature, the range of densities where the entropy per site is sensitive to U continues to shrink. At high temperatures, the charge excitations are important and losing those excitations upon increase of U has more impact on the entropy than the increase of spin excitations so, for densities around 1, the entropy decreases as U is raised up to large values.

Having discussed the entropy per site in the homogeneous model, we can understand the behavior in Fig. 12 more easily. Let us start by the largest volume ($V/N = 0.6$). In

this case, the site occupations are smaller than 1 over the whole trap. Increasing U at relatively small temperatures, we should expect increase of entropy at constant temperature. Therefore, the temperatures lowers to keep the entropy constant. Compressing the system, we will have densities larger than 1 at the center of the trap with small U . In the case of small temperatures, we still expect increase of entropy at constant temperature and, accordingly, decrease of temperature at constant entropy. For larger temperatures with charge excitations present, depending on the density profile, the increase of U can give rise to the opposite behavior, increase of temperature at constant entropy. This must happen if a considerable part of the system has density $n \gtrsim 1$, a situation the system is driven to when the densities larger than 1 in the center of trap are lowered to avoid excessive double occupation upon increase of U . This is illustrated in Fig. 13(d), where the changes in the density profile and temperature during the isentropic change of U for $S/N = 0.9k_B$ and $V/N = 0.4$ can be correlated. The increase of temperature is not expected to continue too far because, for very large U s, the charge excitations will be completely suppressed. The nonmonotonic behavior of the temperature becomes more pronounced as the system volume decreases. This follows

from the fact that under strong compression and small U , there is a large number of particles in the center of the trap where the density becomes very large. Upon increase of U , this large number of particles will spread and give rise to large plateaus, amplifying the effect. Since the density with small U is very large in the center of the trap, densities close to 1 will be achieved only for relatively large values of U , which implies that the nonmonotonic behavior will be observed at larger temperatures compared to what happens in less compressed systems. This is very clear in Fig. 12. Nonmonotonic behavior of the temperature as a function of the intrasite interaction at constant entropy and volume was reported for the two-dimensional system [38,42] but with oscillations in the temperature smaller than we see for the one-dimensional model.

C. Fraction of doubly occupied sites

We finish this section discussing the behavior of the number of doubly occupied sites (N_D) or, alternatively, the fraction of particles in doubly occupied sites,

$$d = \frac{2N_D}{N}, \quad (63)$$

that is an intensive property. In the top panel of Fig. 14 we have the fraction d as a function of temperature and volume per particle for a system with $U = 6.0$. At low temperatures, as the system is compressed starting from large volumes, the fraction d remains small and increases slowly, because the site occupations are small (< 1). The relation between d and density for the homogeneous system can be seen in Fig. 3(b). Due to the energy gap at half-filling, at some point a central plateau with half-filled sites is formed and starts to grow (see the dashed lines in Fig. 10), preventing d of growing faster. d remains increasing slowly until the point where the density in the center of the trap becomes larger than 1. Now, the fraction d starts to grow fast, being energetically advantageous increasing the site occupation in the center of the trap. This fast change in the increasing rate of the fraction d reflects the presence of a Mott insulating phase in the central portion of the trap that started to be destroyed from the center. As we consider compressions at larger temperatures, it is easier to overcome the energy gap and the fast change in the increasing rate of d is gradually smoothed. This is also illustrated in the bottom panel of Fig. 14.

The temperature dependence of the fraction d can be discussed in connection with Figs. 3(b) and 12. From the Helmholtz free-energy differential

$$dF = -SdT - pdV + \mu dN + N_D dU, \quad (64)$$

we have the Maxwell relation

$$\left(\frac{\partial N_D}{\partial T}\right)_{U,V,N} = -\left(\frac{\partial S}{\partial U}\right)_{T,V,N}, \quad (65)$$

which gives us

$$\left(\frac{\partial d}{\partial T}\right)_{U,V,N} = -2\left(\frac{\partial s}{\partial U}\right)_{T,V,N}. \quad (66)$$

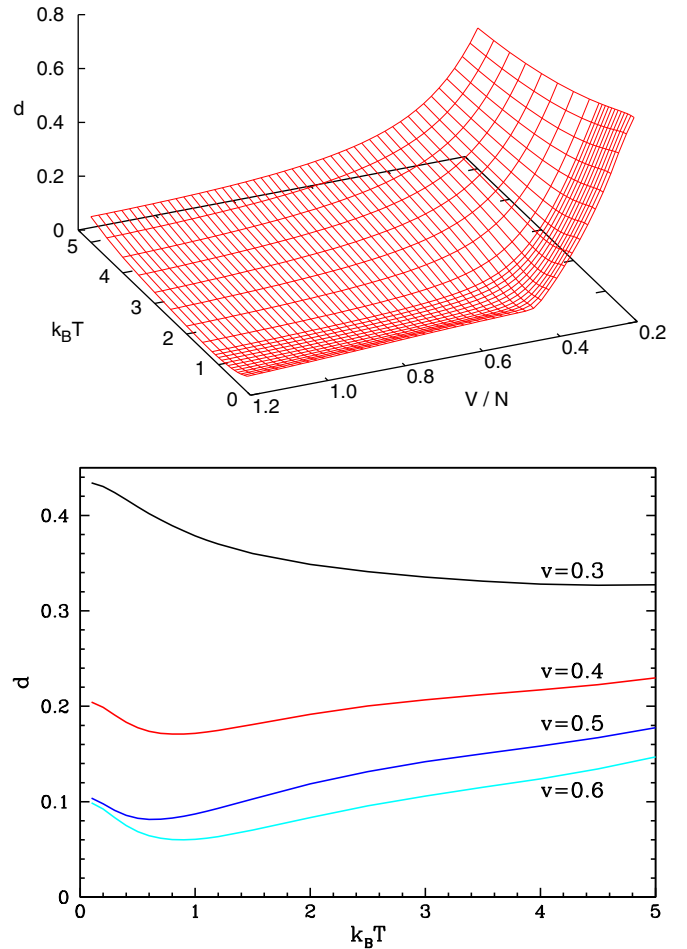


FIG. 14. (Color online) Top panel: Behavior of the fraction d of particles in doubly occupied sites as a function of temperature and volume per particle. Bottom panel: Dependence of the fraction d on temperature for some values of volume per particle.

The right-hand side of Eq. (66) can be rewritten as

$$-\left(\frac{\partial s}{\partial U}\right)_{T,V,N} = \left(\frac{\partial s}{\partial T}\right)_{U,V,N} \left(\frac{\partial T}{\partial U}\right)_{S,V,N}, \quad (67)$$

leading to

$$\left(\frac{\partial d}{\partial T}\right)_{U,V,N} = \frac{2c_v}{T} \left(\frac{\partial T}{\partial U}\right)_{S,V,N}. \quad (68)$$

From Fig. 12 we can qualitatively describe the behavior of d as a function of the temperature. Typically, at low temperatures, d will be a decreasing function of temperature, since $\left(\frac{\partial T}{\partial U}\right)_{S,V,N}$ will be negative in general as discussed above. Depending on U and volume per particle, d will start to increase with the temperature at some point. This behavior is exactly what is seen in the bottom panel of Fig. 14. Consider the particular case of $v = V/N = 0.5$. For $U = 6.0$, below $k_B T = 0.2$, we see from Fig. 10 that the density profile presents a central plateau with half-filled sites. As the temperature is increased, some particles have enough energy to go further away from the center, the central plateau shrinks, and the density in the borders of the trap increases. This effect of course causes the decrease of double occupation. Besides this fact, the increase

of temperature when it is much smaller than the gap (≈ 2.89 , for $U = 6.0$) activates spin excitations, which do not contribute to double occupancy. Accordingly, d decreases. This effect is clear in Fig. 3(b). When the temperature overpass 0.2, a small jump with density slightly greater than one appears in the center of the trap. There are now lateral plateaus. But density also increases in the borders of the trap. The lateral plateaus are shrinking due to particle migration to the center and to the borders. The migration to the center promotes increase of double occupancy, while the migration to the borders promotes decrease of double occupancy. For temperatures still much smaller than the energy gap, the activation of spin excitations dominates, contributing to the decrease of double occupancy. However, at some temperature, charge excitations contributing to increase double occupancy will become important [see also Fig. 3(b)] as well as the migration of particles to the center of the trap will become more intense, making the double occupancy achieve a minimum and then start to increase. For larger temperatures, the lateral plateaus are completely destroyed. Charge excitations become more important and the double occupancy grows. Increasing the temperature now makes the density profile spread out, with particle migration to the borders. This migration tends to decrease double occupation and competes with the charge excitations. The fraction d for a homogeneous model with density n approaches $n^2/2$ (the noninteracting value) as $k_B T \rightarrow \infty$. Therefore, at some high temperature (larger than the gap), the depletion effect will dominate and d will decrease with the temperature, following the behavior of the noninteracting system.

VII. CONCLUSION

In this work we have presented in detail a DFT approach to the thermodynamics of the inhomogeneous one-dimensional Hubbard model. The approach is based on the LDA for the correlation Helmholtz free-energy, where the data for the homogeneous model comes from numerical solution of QTM integral equations [23–25]. The general formalism can be used with any external potential. Extensive comparison between TBALDA and exact diagonalization was done for a small system and TBALDA performed well, allowing its use to study the thermodynamics of larger inhomogeneous systems with smoother confining potentials, where TBALDA must perform even better.

The thermodynamics for the fermionic one-dimensional Hubbard model confined by a parabolic external potential was studied. After introducing the system volume, the trap pressure was obtained, being equal to twice the external potential energy per unit of volume. The thermodynamic description of the confined system was shown to proceed in the same way we classically describe the thermodynamics of a homogeneous system. One must note that the approach used here to treat the one-dimensional model could naturally be used to treat the Hubbard model in two and three dimensions. In these

cases, however, we would have a practical difficulty to make computations based on DFT with LDA, because there is no exact solution for the homogeneous model as it happens in one dimension. Alternative considerations are required to build the energy functionals and this is ongoing research. It is also valid to note that other forms of external potential would lead to a similar thermodynamic description in terms of a volume appropriately defined. For example, with potentials of type $V(x) = |x/L|^p$, we could also define the volume by $2L$ and easily find the meaning of the trap pressure.

The combination of reasonable accuracy and fast computation is the most appealing feature of a DFT approach. The procedure is not exact due to the necessary approximation to build the correlation energy functional, but the errors are typically small enough to let us use it with confidence. The DFT approach based on TBALDA allowed us to determine the thermodynamic properties of the harmonically confined Hubbard model. In this work we emphasized the behavior of the confined system at constant entropy due to the experimental motivation. The whole scenario of isentropic transformations changing the volume or the intrasite interaction was discussed looking at the behavior of the temperature. The necessary conditions to have a trap presenting a Mott-insulator phase were discussed. We found an unusual increase of temperature under isentropic expansion, that can be of experimental interest as well as can motivate new calculations using more precise but much more demanding computational techniques, as QMC, DMRG, or exact diagonalization. The unusual increase of temperature was understood as a consequence of the peculiar density dependence of the correlation entropy per site for the homogeneous model around half-filling at low temperatures. It is possible that this anomalous behavior be a feature of the one-dimensional system only. The nonmonotonic behavior of the temperature under isentropic behavior of U was studied in detail. Such behavior has also been observed to happen in the two-dimensional model [38,42], but it is more prominent in the one-dimensional case. We finished discussing the general behavior of the fraction of particles in doubly occupied sites as a function of temperature and volume per particle showing results in agreement with what could be analyzed from the temperature dependence on interaction during isentropic transformations.

This work opens the door to study, in the framework of DFT, the thermodynamics of the inhomogeneous fermionic one-dimensional Hubbard model in other physically interesting conditions, such as with attractive intrasite interaction and with spin polarization.

ACKNOWLEDGMENTS

The author is grateful to L. N. Oliveira for a careful reading of the manuscript. Financial support from Brazilian agency Conselho Nacional de Desenvolvimento Científico e Tecnológico (CNPq) is acknowledged.

-
- [1] R. G. Parr and W. Yang, *Density-Functional Theory of Atoms and Molecules* (Oxford University Press, Oxford, 1989); W. Kohn, *Rev. Mod. Phys.* **71**, 1253 (1999).
 [2] P. Hohenberg and W. Kohn, *Phys. Rev.* **136**, B864 (1964).

- [3] N. D. Mermin, *Phys. Rev.* **137**, A1441 (1965).
 [4] S. Baroni, S. de Gironcoli, A. Dal Corso, and P. Giannozzi, *Rev. Mod. Phys.* **73**, 515 (2001).

- [5] S. Baroni, P. Giannozzi, and E. Isaev, *Rev. Mineral. Geochem.* **71**, 39 (2010).
- [6] M. C. Payne, M. P. Teter, D. C. Allan, T. A. Arias, and J. D. Joannopoulos, *Rev. Mod. Phys.* **64**, 1045 (1992).
- [7] M. E. Tuckerman, *J. Phys.: Condens. Matter* **14**, R1297 (2002).
- [8] D. Marx and J. Hutter, *Ab Initio Molecular Dynamics: Basic Theory and Advanced Methods* (Cambridge University Press, New York, 2009).
- [9] R. M. Wentzcovitch, Y. G. Yu, and Z. Wu, *Rev. Mineral. Geochem.* **71**, 59 (2010).
- [10] M. P. Desjarlais, J. D. Kress, and L. A. Collins, *Phys. Rev. E* **66**, 025401(R) (2002).
- [11] T. Hickel, B. Grabowski, F. Körmann, and J. Neugebauer, *J. Phys.: Condens. Matter* **24**, 053202 (2012).
- [12] E. W. Brown, B. K. Clark, J. L. DuBois, and D. M. Ceperley, *Phys. Rev. Lett.* **110**, 146405 (2013).
- [13] V. V. Karasiev, T. Sjostrom, J. Dufty, and S. B. Trickey, *Phys. Rev. Lett.* **112**, 076403 (2014).
- [14] K. Capelle and V. L. Campo, *Phys. Rep.* **528**, 91 (2013).
- [15] G. Stefanucci and S. Kurth, *Phys. Rev. Lett.* **107**, 216401 (2011).
- [16] X. Gao, A.-H. Chen, I. V. Tokatly, and S. Kurth, *Phys. Rev. B* **86**, 235139 (2012).
- [17] I. Bloch, J. Dalibard, and W. Zwerger, *Rev. Mod. Phys.* **80**, 885 (2008).
- [18] P. M. Duarte, R. A. Hart, T.-L. Yang, X. Liu, T. Paiva, E. Khatami, R. T. Scalettar, N. Trivedi, and R. G. Hulet, *Phys. Rev. Lett.* **114**, 070403 (2015).
- [19] R. A. Hart, P. M. Duarte, T.-L. Yang, X. Liu, T. Paiva, E. Khatami, R. T. Scalettar, N. Trivedi, D. A. Huse, and R. G. Hulet, *Nature (London)* **519**, 211 (2015).
- [20] M. Takahashi, *Prog. Theor. Phys.* **47**, 69 (1972).
- [21] M. Takahashi, *Thermodynamics of One-Dimensional Solvable Models* (Cambridge University Press, Cambridge, 1999).
- [22] M. Takahashi and M. Shiroishi, *Phys. Rev. B* **65**, 165104 (2002).
- [23] A. Klümper and R. Z. Bariev, *Nucl. Phys. B* **458**, 623 (1996).
- [24] G. Jüttner, A. Klümper, and J. Suzuki, *Nucl. Phys. B* **522**, 471 (1998).
- [25] F. H. L. Essler, F. Holger, F. Göhmann, A. Klümper, and V. E. Korepin, *The One-Dimensional Hubbard Model* (Cambridge University Press, Cambridge, 2005).
- [26] M. Rigol, A. Muramatsu, G. G. Batrouni, and R. T. Scalettar, *Phys. Rev. Lett.* **91**, 130403 (2003).
- [27] X.-J. Liu, P. D. Drummond, and H. Hu, *Phys. Rev. Lett.* **94**, 136406 (2005).
- [28] N. A. Lima, L. N. Oliveira, and K. Capelle, *Europhys. Lett.* **60**, 601 (2002).
- [29] N. A. Lima, M. F. Silva, L. N. Oliveira, and K. Capelle, *Phys. Rev. Lett.* **90**, 146402 (2003).
- [30] G. Xianlong, M. Polini, M. P. Tosi, V. L. Campo, K. Capelle, and M. Rigol, *Phys. Rev. B* **73**, 165120 (2006).
- [31] W. Kohn and L. J. Sham, *Phys. Rev.* **140**, A1133 (1965).
- [32] R. Lopez-Sandoval and G. M. Pastor, *Phys. Rev. B* **69**, 085101 (2004).
- [33] K. Capelle and L. N. Oliveira, *Phys. Rev. B* **73**, 113111 (2006).
- [34] A. Akande, *Braz. J. Phys.* **44**, 215 (2014).
- [35] M. Ijäs and A. Harju, *Phys. Rev. B* **82**, 235111 (2010).
- [36] D. Karlsson, A. Privitera, and C. Verdozzi, *Phys. Rev. Lett.* **106**, 116401 (2011).
- [37] T. Paiva, Y. L. Loh, M. Randeria, R. T. Scalettar, and N. Trivedi, *Phys. Rev. Lett.* **107**, 086401 (2011).
- [38] E. Khatami and M. Rigol, *Phys. Rev. A* **84**, 053611 (2011).
- [39] E. V. Gorelik, D. Rost, T. Paiva, R. Scalettar, A. Klümper, and N. Blümer, *Phys. Rev. A* **85**, 061602 (2012).
- [40] V. L. Campo, K. Capelle, C. Hooley, J. Quintanilla, and V. W. Scarola, *Phys. Rev. A* **85**, 033644 (2012).
- [41] B. Tang, T. Paiva, E. Khatami, and M. Rigol, *Phys. Rev. Lett.* **109**, 205301 (2012).
- [42] B. Tang, T. Paiva, E. Khatami, and M. Rigol, *Phys. Rev. B* **88**, 125127 (2013).
- [43] Zu-Jian Ying, V. Brosco and J. Lorenzana, *Phys. Rev. B* **89**, 205130 (2014).
- [44] See Supplemental Material at <http://link.aps.org/supplemental/10.1103/PhysRevA.92.013614> for simple cross checking of method implementation.
- [45] N. A. Lima, A. L. Malvezzi, and K. Capelle, *Solid State Commun.* **144**, 557 (2007).
- [46] B. Sciola, A. Tokuno, S. Uchino, P. Barmettler, T. Giamarchi, and C. Kollath, *Phys. Rev. A* **88**, 063629 (2013).
- [47] V. L. Campo, J. Quintanilla, and C. Hooley, *Physica B* **404**, 3328 (2009).
- [48] J. Voit, *Rep. Prog. Phys.* **58**, 977 (1995).